



CERN-PPE/92-143
31 August 1992

**Measurement of Prompt Photon Production
in Hadronic Z decays**

The ALEPH Collaboration*

Abstract

The production of isolated photons in hadronic Z decays is measured with the ALEPH detector at LEP using a sample of 450,000 hadronic events. The corrected rate is given for several values of the minimum invariant mass squared cut between the photon and the jets. This measurement of final state radiation from the quarks is compared with the predictions of parton shower models JETSET, ARIADNE and HERWIG as well as with the predictions of QCD matrix element calculations.

(Submitted to Zeitschrift für Physik C)

*See the following pages for the list of authors.

The ALEPH Collaboration

D. Buskulic, D. Decamp, C. Goy, J.-P. Lees, M.-N. Minard, B. Mours

Laboratoire de Physique des Particules (LAPP), IN²P³-CNRS, 74019 Annecy-le-Vieux Cedex, France

R. Alemany, F. Ariztizabal, P. Comas, J.M. Crespo, M. Delfino, E. Fernandez, V. Gaitan, Ll. Garrido, A. Pacheco, A. Pascual

Institut de Fisica d'Altes Energies, Universitat Autònoma de Barcelona, 08193 Bellaterra (Barcelona), Spain⁸

D. Creanza, M. de Palma, A. Farilla, G. Iaselli, G. Maggi, M. Maggi, S. Natali, S. Nuzzo, M. Quattromini, A. Ranieri, G. Raso, F. Romano, F. Ruggieri, G. Selvaggi, L. Silvestris, P. Tempesta, G. Zito

INFN Sezione di Bari e Dipartimento di Fisica dell'Università, 70126 Bari, Italy

H. Hu,²¹ D. Huang, X. Huang, J. Lin, J. Lou, C. Qiao,²¹ T. Wang, Y. Xie, D. Xu, R. Xu, J. Zhang, W. Zhao

Institute of High-Energy Physics, Academia Sinica, Beijing, The People's Republic of China⁹

W.B. Atwood,² L.A.T. Bauerdick,²⁵ E. Blucher, G. Bonvicini, F. Bossi, J. Boudreau, T.H. Burnett,³ H. Drevermann, R.W. Forty, R. Hagelberg, J. Harvey, S. Haywood, J. Hilgart, R. Jacobsen, B. Jost, J. Knobloch, E. Lançon, I. Lehraus, T. Lohse, A. Lusiani, M. Martinez, P. Mato, T. Mattison, H. Meinhard, S. Menary,²⁶ A. Minten, R. Miquel, H.-G. Moser, P. Palazzi, J.A. Perlas, J.-F. Puztaszeri,³⁵ F. Ranjard, G. Redlinger,²⁷ L. Rolandi, A. Roth,²⁸ J. Rothberg,³ T. Ruan,^{21,31} M. Saich, D. Schlatter, M. Schmelling, F. Sefkow, W. Tejessy, H. Wachsmuth, W. Wiedenmann, T. Wildish, W. Witzeling, J. Wotschack

European Laboratory for Particle Physics (CERN), 1211 Geneva 23, Switzerland

Z. Ajaltouni, F. Badaud, M. Bardadin-Otwinowska, A.M. Bencheikh, R. El Fellous, A. Falvard, P. Gay, C. Guicheney, P. Henrard, J. Jousset, B. Michel, J.-C. Montret, D. Pallin, P. Perret, B. Pietrzyk, J. Prorini, F. Prulhière, G. Stimpf

Laboratoire de Physique Corpusculaire, Université Blaise Pascal, IN²P³-CNRS, Clermont-Ferrand, 63177 Aubière, France

T. Fearnley, J.D. Hansen, J.R. Hansen,¹ P.H. Hansen, R. Møllerud, B.S. Nilsson

Niels Bohr Institute, 2100 Copenhagen, Denmark¹⁰

I. Efthymiopoulos, A. Kyriakis, E. Simopoulou, A. Vayaki,¹ K. Zachariadou

Nuclear Research Center Demokritos (NRCD), Athens, Greece

J. Badier, A. Blondel, G. Bonneaud, J.C. Brient, G. Fouque, S. Orteu, A. Rosowsky, A. Rougé, M. Rumpf, R. Tanaka, M. Verderi, H. Videau

Laboratoire de Physique Nucléaire et des Hautes Energies, Ecole Polytechnique, IN²P³-CNRS, 91128 Palaiseau Cedex, France

D.J. Candlin, M.I. Parsons, E. Veitch

Department of Physics, University of Edinburgh, Edinburgh EH9 3JZ, United Kingdom¹¹

L. Moneta, G. Parrini

Dipartimento di Fisica, Università di Firenze, INFN Sezione di Firenze, 50125 Firenze, Italy

M. Corden, C. Georgiopoulos, M. Ikeda, J. Lannutti, D. Levinthal,¹⁶ M. Mermikides[†], L. Sawyer, S. Wasserbaech
Supercomputer Computations Research Institute and Dept. of Physics, Florida State University, Tallahassee, FL 32306, USA^{13,14,15}

A. Antonelli, R. Baldini, G. Bencivenni, G. Bologna,⁵ P. Campana, G. Capon, F. Cerutti, V. Chiarella, B. D'Ettorre-Piazzoli,³⁰ G. Felici, P. Laurelli, G. Mannocchi,⁶ F. Murtas, G.P. Murtas, L. Passalacqua, M. Pepe-Altarelli, P. Picchi⁵

Laboratori Nazionali dell'INFN (LNF-INFN), 00044 Frascati, Italy

B. Altoon, O. Boyle, P. Colrain, I. ten Have, J.G. Lynch, W. Maitland, W.T. Morton, C. Raine, J.M. Scarr, K. Smith, A.S. Thompson, R.M. Turnbull

Department of Physics and Astronomy, University of Glasgow, Glasgow G12 8QQ, United Kingdom¹¹

B. Brandl, O. Braun, R. Geiges, C. Geweniger, P. Hanke, V. Hepp, E.E. Kluge, Y. Maumary, A. Putzer, B. Rensch, A. Stahl, K. Tittel, M. Wunsch

Institut für Hochenergiephysik, Universität Heidelberg, 6900 Heidelberg, Fed. Rep. of Germany¹⁷

A.T. Belk, R. Beuselinck, D.M. Binnie, W. Cameron, M. Cattaneo, D.J. Colling, P.J. Dornan,¹ S. Dugeay, A.M. Greene, J.F. Hassard, N.M. Lieske, J. Nash, S.J. Patton, D.G. Payne, M.J. Phillips, J.K. Sedgbeer, I.R. Tomalin, A.G. Wright

Department of Physics, Imperial College, London SW7 2BZ, United Kingdom¹¹

E. Kneringer, D. Kuhn, G. Rudolph

Institut für Experimentalphysik, Universität Innsbruck, 6020 Innsbruck, Austria¹⁹

C.K. Bowdery, T.J. Brodbeck, A.J. Finch, F. Foster, G. Hughes, D. Jackson, N.R. Keemer, M. Nuttall, A. Patel, T. Sloan, S.W. Snow, E.P. Whelan

Department of Physics, University of Lancaster, Lancaster LA1 4YB, United Kingdom¹¹

K. Kleinknecht, J. Raab, B. Renk, H.-G. Sander, H. Schmidt, F. Steeg, S.M. Walther, B. Wolf

Institut für Physik, Universität Mainz, 6500 Mainz, Fed. Rep. of Germany¹⁷

J.-J. Aubert, C. Benchouk, A. Bonissent, J. Carr, P. Coyle, J. Drinkard, F. Etienne, S. Papalexioiu, P. Payre, Z. Qian, L. Roos, D. Rousseau, P. Schwemling, M. Talby

Centre de Physique des Particules, Faculté des Sciences de Luminy, IN²P³-CNRS, 13288 Marseille, France

S. Adlung, C. Bauer, W. Blum,¹ D. Brown, G. Cowan, B. Dehning, H. Dietl, F. Dydak,²⁴ M. Fernandez-Bosman, M. Frank, A.W. Halley, J. Lauber, G. Lütjens, G. Lutz, W. Männer, R. Richter, H. Rotscheidt, J. Schröder, A.S. Schwarz, R. Settles, H. Seywerd, U. Stierlin, U. Stiegler, R. St. Denis, M. Takashima,⁴ J. Thomas,⁴ G. Wolf

Max-Planck-Institut für Physik, Werner-Heisenberg-Institut, 8000 München, Fed. Rep. of Germany¹⁷

V. Bertin, J. Boucrot, O. Callot, X. Chen, A. Cordier, M. Davier, J.-F. Grivaz, Ph. Heusse, P. Janot, D.W. Kim,²⁰ F. Le Diberder, J. Lefrançois, A.-M. Lutz, M.-H. Schune, J.-J. Veillet, I. Videau, Z. Zhang, F. Zomer

Laboratoire de l'Accélérateur Linéaire, Université de Paris-Sud, IN²P³-CNRS, 91405 Orsay Cedex, France

D. Abbaneo, S.R. Amendolia, G. Bagliesi, G. Batignani, L. Bosisio, U. Bottigli, C. Bradaschia, M. Carpinelli, M.A. Ciocci, R. Dell'Orso, I. Ferrante, F. Fidecaro, L. Foà, E. Focardi, F. Forti, A. Giassi, M.A. Giorgi, F. Ligabue, E.B. Mannelli, P.S. Marrocchesi, A. Messineo, F. Palla, G. Rizzo, G. Sanguinetti, J. Steinberger, R. Tenchini, G. Tonelli, G. Triggiani, C. Vannini, A. Venturi, P.G. Verdini, J. Walsh

Dipartimento di Fisica dell'Università, INFN Sezione di Pisa, e Scuola Normale Superiore, 56010 Pisa, Italy

J.M. Carter, M.G. Green, P.V. March, Ll.M. Mir, T. Medcalf, I.S. Quazi, J.A. Strong, L.R. West

Department of Physics, Royal Holloway & Bedford New College, University of London, Surrey TW20 OEX, United Kingdom¹¹

D.R. Botterill, R.W. Clift, T.R. Edgecock, M. Edwards, S.M. Fisher, T.J. Jones, P.R. Norton, D.P. Salmon, J.C. Thompson

Particle Physics Dept., Rutherford Appleton Laboratory, Chilton, Didcot, Oxon OX11 0QX, United Kingdom¹¹

B. Bloch-Devaux, P. Colas, H. Duarte, W. Kozanecki, M.C. Lemaire, E. Locci, S. Loucatos, E. Monnier, P. Perez, F. Perrier, J. Rander, J.-F. Renardy, A. Roussarie, J.-P. Schuller, J. Schwindling, D. Si Mohand, B. Vallage

*Service de Physique des Particules, DAPNIA, CE-Saclay, 91191 Gif-sur-Yvette Cedex, France*¹⁸

R.P. Johnson, A.M. Litke, G. Taylor, J. Wear

*Institute for Particle Physics, University of California at Santa Cruz, Santa Cruz, CA 95064, USA*³⁴

J.G. Ashman, W. Babbage, C.N. Booth, C. Büttar, R.E. Carney, S. Cartwright, F. Combley, F. Hatfield, P. Reeves, L.F. Thompson¹

*Department of Physics, University of Sheffield, Sheffield S3 7RH, United Kingdom*¹¹

E. Barberio, A. Böhrer, S. Brandt, C. Grupen, L. Mirabito,²⁹ F. Rivera, U. Schäfer

*Fachbereich Physik, Universität Siegen, 5900 Siegen, Fed. Rep. of Germany*¹⁷

G. Ganis,³³ G. Giannini, B. Gobbo, F. Ragusa²³

Dipartimento di Fisica, Università di Trieste e INFN Sezione di Trieste, 34127 Trieste, Italy

L. Bellantoni, W. Chen, D. Cinabro,³² J.S. Conway, D.F. Cowen,²² Z. Feng, D.P.S. Ferguson, Y.S. Gao, J. Grahl, J.L. Harton, R.C. Jared,⁷ B.W. LeClaire, C. Lishka, Y.B. Pan, J.R. Pater, Y. Saadi, V. Sharma, M. Schmitt, Z.H. Shi, A.M. Walsh, F.V. Weber, M.H. Whitney, Sau Lan Wu, X. Wu, G. Zobernig

*Department of Physics, University of Wisconsin, Madison, WI 53706, USA*¹²

† Deceased.

¹ Now at CERN, PPE Division, 1211 Geneva 23, Switzerland.

² Permanent address: SLAC, Stanford, CA 94309, USA

³ Permanent address: University of Washington, Seattle, WA 98195, USA.

⁴ Now at SSCL, Dallas, TX, U.S.A.

⁵ Also Istituto di Fisica Generale, Università di Torino, Torino, Italy.

⁶ Also Istituto di Cosmo-Geofisica del C.N.R., Torino, Italy.

⁷ Permanent address: LBL, Berkeley, CA 94720, USA.

⁸ Supported by CICYT, Spain.

⁹ Supported by the National Science Foundation of China.

¹⁰ Supported by the Danish Natural Science Research Council.

¹¹ Supported by the UK Science and Engineering Research Council.

¹² Supported by the US Department of Energy, contract DE-AC02-76ER00881.

¹³ Supported by the US Department of Energy, contract DE-FG05-87ER40319.

¹⁴ Supported by the NSF, contract PHY-8451274.

¹⁵ Supported by the US Department of Energy, contract DE-FC05-85ER250000.

¹⁶ Supported by SLOAN fellowship, contract BR 2703.

¹⁷ Supported by the Bundesministerium für Forschung und Technologie, Fed. Rep. of Germany.

¹⁸ Supported by the Direction des Sciences de la Matière, C.E.A.

¹⁹ Supported by Fonds zur Förderung der wissenschaftlichen Forschung, Austria.

²⁰ Supported by the Korean Science and Engineering Foundation and Ministry of Education.

²¹ Supported by the World Laboratory.

²² Now at California Institute of Technology, Pasadena, CA 91125, USA.

²³ Now at Dipartimento di Fisica, Università di Milano, Milano, Italy.

²⁴ Also at CERN, PPE Division, 1211 Geneva 23, Switzerland.

²⁵ Now at DESY, Hamburg, Germany.

²⁶ Now at University of California at Santa Barbara, Santa Barbara, CA 93106, USA.

²⁷ Now at TRIUMF, Vancouver, B.C., Canada.

²⁸ Now at Lufthansa, Hamburg, Germany.

²⁹ Now at Institut de Physique Nucléaire de Lyon, 69622 Villeurbanne, France.

³⁰ Also at Università di Napoli, Dipartimento di Scienze Fisiche, Napoli, Italy.

³¹ On leave of absence from IHEP, Beijing, The People's Republic of China.

³² Now at Harvard University, Cambridge, MA 02138, U.S.A.

³³ Supported by the Consorzio per lo Sviluppo dell'Area di Ricerca, Trieste, Italy.

³⁴ Supported by the US Department of Energy, grant DE-FG03-92ER40689.

³⁵ Visitor from University of Wisconsin, Madison, WI 53706, USA.

1 Introduction

The main source of isolated photons in hadronic decays of the Z in e^+e^- annihilation is final state radiation (FSR) from quarks. Since the properties of the radiated photons reflect the properties of the radiating quarks, energetic FSR photons provide a unique probe of the early parton showering mechanism free of fragmentation effects [1]. Thus, a detailed study of FSR appears as a test of QCD phenomenology [2].

In perturbative QCD, matrix element calculations of the FSR rate have been made up to $O(\alpha_s)$ [3,4,5] corresponding to the emission of one gluon and one photon at tree level. The cross-sections are given in terms of the scaled invariant mass squared variable y_{cut} between the photon and the partons, enabling also the jet topology of the whole associated event to be determined. These calculations have now been implemented in a Monte-Carlo framework, allowing a better comparison with the available data [4,6].

An alternative to fixed order matrix element calculations which quickly become prohibitive for higher orders, is given by parton shower models. In these models, the conversion of the primary partons into hadrons is described by a probabilistic cascade which effectively sums up all leading terms and part of the next-to-leading terms of the perturbative expansion. The models differ in the implementation of next-to-leading and sub-leading terms. Three parton shower models which include FSR photon production are studied in this work : JETSET 7.3 [7], ARIADNE 4.2 [8] and HERWIG 5.4 [9].

Each parton shower model simulates the partonic cascade by a semi-classical algorithm based on elementary branching processes. The elementary branching of partons can be formulated in terms of perturbative QCD splitting functions as in JETSET and HERWIG or in terms of colour dipole splitting as in ARIADNE. In addition, in order to account for interference effects [10], an ordering condition is imposed on subsequent branchings, either in terms of transverse momenta as in ARIADNE or in terms of emission angles as in JETSET or in HERWIG. Each parton shower model has parameters whose values are fixed by adjusting them to reproduce the inclusive charged particle distributions and the event shape variables in hadronic Z decays [11]. This leaves no more free parameters with which to adjust the photon emission. Since it has been shown that the predictions from the parton shower models for the FSR photon rate differ [2], a comparison with the data might ultimately discriminate between the various parton shower models and lead to a better understanding of the mechanisms of parton cascades.

The measurement presented in this paper is based on a sample of 447,706 hadronic Z decays collected in 1989, 1990 and 1991 at centre of mass energies between 88 GeV and 95 GeV, corresponding to an integrated luminosity of 19.8pb^{-1} .

Following an earlier ALEPH publication based upon only 180,000 hadronic events [12], this paper presents a detailed comparison of the measured FSR photon properties with the parton shower models and matrix element calculations. The comparison is extended to individual jet topologies in terms of the y_{cut} variable.

The outline of this paper is as follows. After the properties of the ALEPH detector have been recalled, the selection of isolated photon candidates in hadronic events and the photon identification method are presented. The subtraction of various background contributions is then described and the systematic errors on the FSR signal are discussed. The parton shower models are presented and a first comparison of their predictions with

the data is given. These models are then used to correct the observed signal for detector and fragmentation effects, allowing the production rate to be compared with predictions at parton level.

2 The ALEPH Detector

The ALEPH detector is described in detail in [13].

Charged particles are detected in an inner tracking drift chamber (ITC) surrounded by a large cylindrical time projection chamber (TPC) inside a 1.5 T superconducting solenoid. Tracks with polar angles θ such that $|\cos \theta| < 0.95$ traverse at least 6 TPC pad rows. The momentum resolution, determined using dimuon events, is $\Delta p/p^2 = 0.8 \cdot 10^{-3}(\text{GeV}/c)^{-1}$. The single track finding efficiency in hadronic events is about 99% for transverse momenta above 200 MeV/c.

Photons and electrons are detected in the electromagnetic calorimeter (ECAL) which surrounds the TPC inside the coil. The calorimeter is instrumented down to polar angles θ such that $|\cos \theta| < 0.98$. It is divided into a barrel and two end-caps, each segmented in azimuth into 12 modules. Each module consists of 45 lead plates interspersed with planes of proportional tubes filled with a mixture of Xe(80%) and CO₂(20%). These plates are grouped in three stacks of 4, 9 and 9 radiation lengths in depth. Ionization in the gas induces charges that are collected on segmented cathode planes ("pads"). The pads from consecutive planes are connected to form projective towers covering an angular region of $0.8^\circ \times 0.8^\circ$ each on average. Each tower is read out in three successive storeys in depth, corresponding to the three stacks. Anode wire signals are summed plane by plane, giving 45 read-out channels per module.

The response of the ECAL to electrons and photons has been studied with $e^+e^- \rightarrow e^+e^-$, $(e^+e^-)e^+e^-$, $e^+e^-\gamma$ and $\mu^+\mu^-\gamma$ events. The energy resolution has been measured in the energy range from 1 GeV to the beam energy to be $(\Delta E/E)^2 = ((2.5 \pm 0.1)\%)^2 + ((19.9 \pm 0.3)\%/\sqrt{E})^2$. The angular resolution is typically $4 \text{ mr}/\sqrt{E}$.

The photon conversion probability in the material in front of the ECAL varies from 4.8% at 90° to the beam axis to 9.0% at 30° to the beam axis. These values, calculated using a simulation of the ALEPH detector, were increased to 6.5% at 90° and 10.5% at 30° when the vertex detector and a new beam pipe were installed in 1991.

The hadron calorimeter (HCAL) has 23 layers of iron absorber interleaved with limited streamer tubes $9 \times 9 \text{ mm}^2$ in cross-section. It is divided into barrel and endcap sub-detectors and has a tower readout similar to the ECAL with towers of angular size about $3.7^\circ \times 3.7^\circ$. The energy resolution of the HCAL is about $80\%/\sqrt{E}$ for hadronic showers.

The ECAL barrel and endcaps are rotated in azimuth by 1.8° relative to the HCAL so that the HCAL modules cover the small gaps ("cracks") between the ECAL modules. Thus, the ALEPH detector is a hermetic fine grained detector well suited for photon detection, particle separation and energy flow measurement in hadronic events, an important feature for the reconstruction of jets.

For each event, the magnitude and the direction of the energy flow is reconstructed by combining the information from all sub-detectors, taking advantage of the redundancy of energy and momentum measurements. The reconstructed "energy flow objects" are

charged particles, V^0 s (long-lived neutral particles decaying into two reconstructed tracks with opposite charges), photons and neutral hadronic energy. The performance of the energy flow algorithm is discussed in [14].

3 The Selection of Isolated Photon Candidates

3.1 The Hadronic Event Selection

A track reconstructed in the ITC/TPC is required to originate from within a cylinder centred on the interaction point, with a 2.5 cm radius from the beam direction and a ± 7 cm length along the beam direction, and to have a polar angle θ such that $|\cos \theta| < 0.95$ and a minimum of 4 reconstructed TPC coordinates. An event must have at least 5 such "good" tracks and the sum of the energies of the tracks must be greater than 10% of the centre of mass energy. In addition, the number of energy flow objects is required to be at least 15 and the visible mass of all energy flow objects is required to be larger than 40% of the centre of mass energy.

The efficiency of this hadronic event selection is determined by a Monte-Carlo simulation to be (97.26 ± 0.06) % with small contaminations of $\tau\tau$ events, (0.042 ± 0.002) % and $\gamma\gamma$ events, (0.08 ± 0.012) %.

The number of events satisfying this hadronic event selection is 447,706 comprising 18,245, 145,805 and 283,656 events respectively from the 1989, 1990 and 1991 data taking. The fraction of events at the Z peak ($\sqrt{s}=91.2$ GeV) is 73%. All hadronic events are examined for isolated photon candidates in the ECAL.

3.2 The Photon Identification

ECAL towers with significant energy deposition are grouped into clusters. Photon candidates are selected from clusters with energy E_γ greater than 5 GeV which are not linked to a reconstructed track in the ITC/TPC ("neutral" clusters).

The polar angle θ_γ of the vector joining the barycentre of the cluster to the centre of the detector must be such that $|\cos \theta_\gamma| \leq 0.95$. When the tower with the maximum energy is at the edge of an ECAL module in azimuth ("crack"), the cluster is eliminated. This condition introduces a 5.5% loss in the barrel and a 6% loss in the endcaps.

The transverse energy of the cluster with respect to the beam axis is required to be larger than 5 GeV. This cut eliminates a region of phase space where initial state radiation (ISR) background is significant.

Clusters which deposit more than 40% of their energy in the third stack of the ECAL (non-electromagnetic clusters) are rejected, thus removing about 55% of clusters originating from long-lived neutral hadrons. The efficiency for this cut to retain photons is measured using a reference sample of 2189 kinematically fitted radiative dimuon and Bhabha events with $E_\gamma > 5$ GeV. The overall efficiency is (98.1 ± 0.3) % but decreases slowly with energy (98.8 ± 0.4) % for $E_\gamma < 10$ GeV and (96.9 ± 1.1) % for $30 < E_\gamma < 40$ GeV).

The separation of single photons from clusters produced by π^0 , η^0 or several unrelated photons employs the transverse shape of the energy deposition. This is characterized by the fraction F_4 of the cluster energy contained in the sub-cluster of 2×2 adjacent towers

with maximum energy (leading sub-cluster) [12]. Using the variable F_4 , a normalised estimator RF_4 is defined :

$$RF_4 = \frac{F_4 - \langle F_4 \rangle}{\sigma_4} \quad (1)$$

where $\langle F_4 \rangle$ and σ_4 are the average and the standard deviation of the F_4 distributions measured with the reference sample of $e e \gamma$ and $\mu \mu \gamma$ events as a function of E_γ and θ_γ .

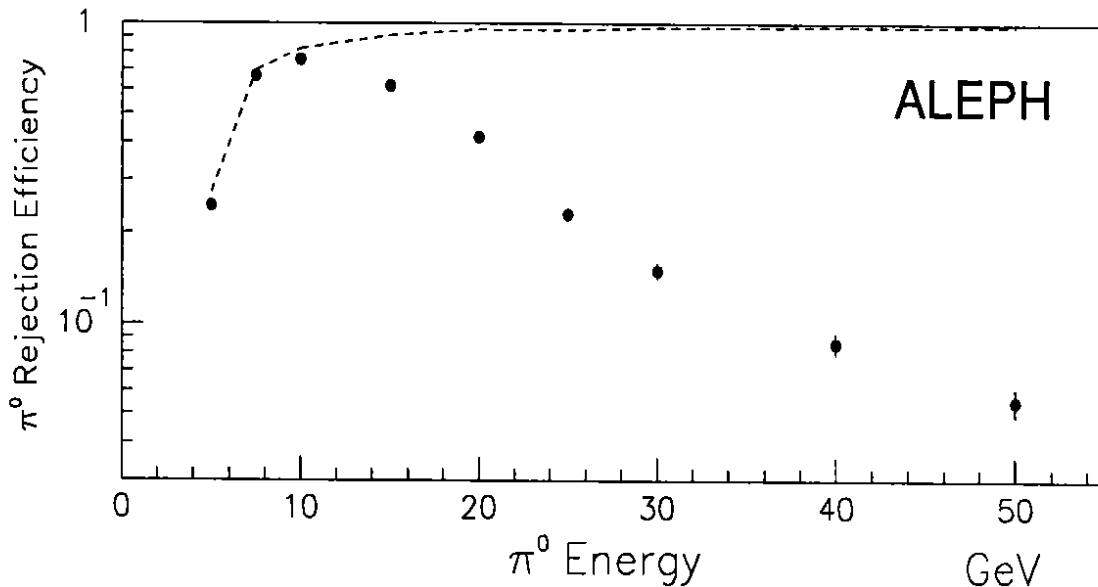


Figure 1: The π^0 rejection efficiency of the photon identification cut $RF_4 > -2$ for π^0 s as a function of the π^0 energy, obtained from a Monte-Carlo simulation of the ALEPH detector. The dashed line represents the probability for a π^0 to produce a single cluster in the ECAL.

Applying a cut $RF_4 > -2$, (94.9 ± 0.5) % of the single photons in the reference sample are retained, independent of energy. The rejection efficiency for π^0 s is calculated using a Monte-Carlo simulation and is plotted in figure 1. The drop of the rejection efficiency at low energy is due to the separation of the two photons from the π^0 into two separate clusters. The cut on RF_4 also removes 95% of the remaining clusters due to long-lived neutral hadrons.

Taking into account the energy and angular distributions of photons in the reference sample, the systematic uncertainty on the photon identification efficiency is estimated to be 1%.

3.3 Isolation

In order to reduce the non-prompt background, the photon candidate is required to be isolated from other particles in the event using a cone of half-angle 20° . It is required that no charged track with momentum greater than 500 MeV is found inside the cone, nor any other ECAL neutral electromagnetic cluster with energy above 500 MeV, nor any neutral HCAL cluster with energy above 2 GeV. Clusters in HCAL are not considered for the

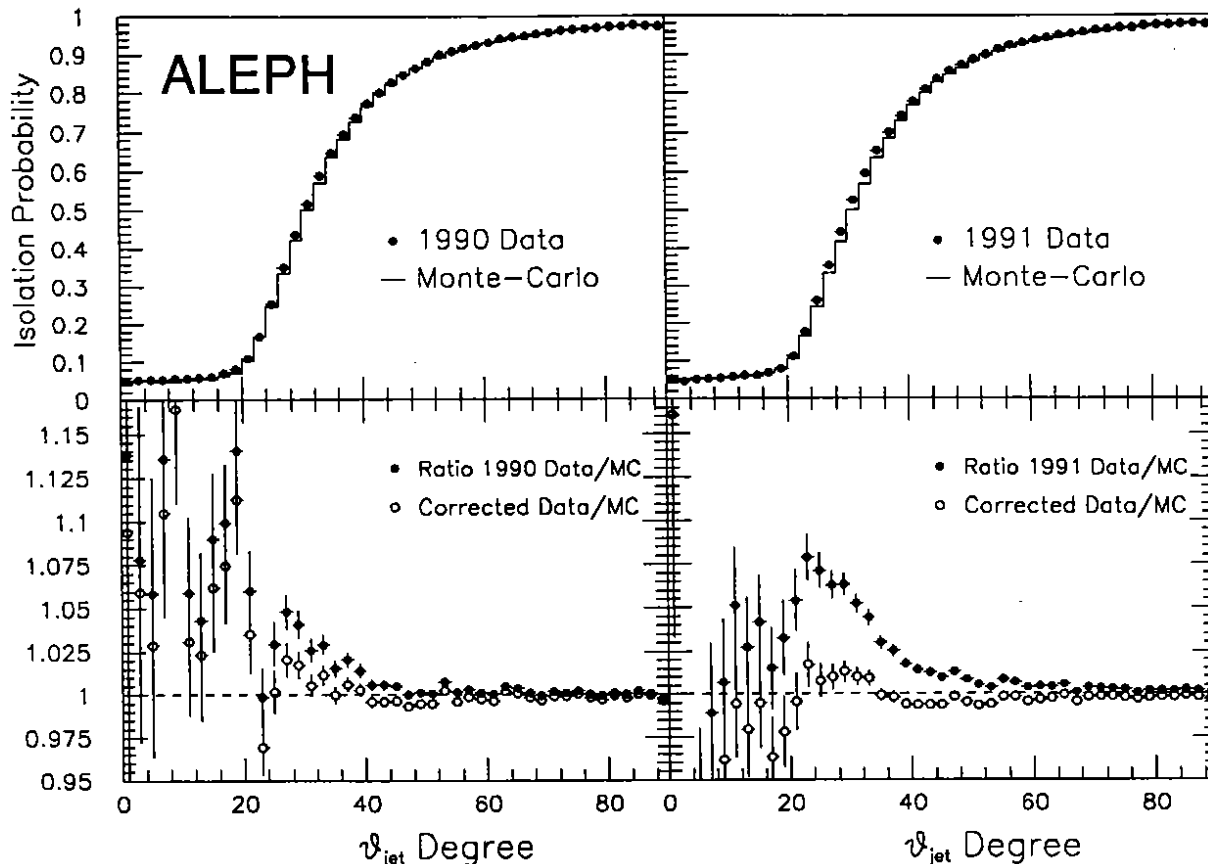


Figure 2: The isolation probability as a function of the angle to the nearest jet measured with random vectors inserted into hadronic events. The full points correspond to the measurements with the 1990 and 1991 data. The histograms refer to the corresponding measurement with the Monte-Carlo. The open points correspond to the modified ratios after the isolation correction.

isolation condition if they are at an angle of less than 2.6° to the photon candidate and if their energy is less than 20 GeV. Otherwise, a small fraction (less than 4%) of photons would be rejected due to energy leakage from the ECAL into the HCAL, close to ECAL cracks.

This definition of isolation by a geometrical cone is sensitive to the distribution of low energy fragments around jets and the presence of noise in the calorimeters. However, these systematic effects can be measured independently by inserting isotropic random vectors representing photons into hadronic events in the data and the simulation [12]. The fraction of random vectors surviving the isolation condition is a measurement of the isolation probability. Comparisons of these probabilities in the data and in the Monte-Carlo simulation are shown in figure 2 as a function of their angle θ_{jet} to the nearest jet. Jets are found by applying the JADE [15] algorithm (E0 recombination scheme) to all energy flow objects using $y_{cut} = 0.01$ and $E_{vis} = \sqrt{s}$. The isolation probability is larger in the data than in the simulation for small θ_{jet} . When using charged tracks only in the 20° cone, the isolation probabilities agree. The observed difference is related to an excess of low energy neutrals in the Monte-Carlo compared with the data. The conclusions of this study do not depend on the value of y_{cut} used for the jet algorithm nor on the angular

distribution used for the random vectors.

This inadequacy of the simulation can be corrected if the thresholds used for neutral ECAL clusters in the 20° cone are adjusted. If a 450 MeV (420 MeV) threshold is taken for the 1990 (1991) data, while the 500 MeV threshold is kept in the simulation, the measured isolation probabilities agree (see figure 2).

The reduction of the thresholds in the data compared with the simulation is referred to later as the "isolation correction". This correction, which depends strongly on θ_{jet} as illustrated in figure 2, corresponds to a reduction of the final number of prompt photons with $E_\gamma > 5$ GeV by 2.0 %. In the following, the isolation correction is taken to be the systematic error coming from the isolation condition.

3.4 The Isolated Photon Candidate Samples

Finally, the isolated photon candidates must satisfy the requirement that their angle θ_{jet} to the nearest jet is larger than 40° . If the energy E_{jet} of the nearest jet is greater than 20 GeV, the cut on θ_{jet} is reduced to 20° . Jets are found by applying the JADE algorithm to energy flow objects as described previously in section 3.3, removing the photon candidate and any associated HCAL cluster. This cut on θ_{jet} and E_{jet} removes low multiplicity jets close to the photon candidate which may not be reproduced well by the simulation and has the advantage of reducing further the non-prompt background.

After all cuts, 1336 isolated photon candidates remain. The number of candidates as a function of energy is given in table 1a.

Reduced samples are defined using the y_{cut} variable in the following way [16]. Jets are reconstructed with the JADE algorithm applied to all energy flow objects for a given y_{cut} , removing the photon candidate and any associated HCAL cluster. A y_γ variable is defined for the photon as :

$$y_\gamma = \min_s \frac{2E_i E_\gamma (1 - \cos \theta_{\gamma-jet i})}{s}$$

where the minimum runs over all jets i in the event, E_i is the energy of jet i and $\theta_{\gamma-jet i}$ is the angle between jet i and the photon candidate. The photon candidate is kept if $y_\gamma > y_{cut}$.

Defined in this way, the y_{cut} variable is a convenient measure of the degree of isolation. The number of candidates as a function of y_{cut} is given in table 1b.

4 Background Subtractions and Systematic Errors

4.1 Initial State Radiation Background

The ISR background is estimated using a high statistics simulation of hadronic events generated with the same \sqrt{s} distribution of the luminosity as the data. Numbers are given in table 1. This background amounts to (5.8 ± 0.5) % for $E_\gamma > 5$ GeV but it is concentrated at low photon energy (9% for $E_\gamma < 10$ GeV) and at very high energy (9% for $E_\gamma > 40$ GeV). The ISR background fraction is almost independent of y_{cut} . The ISR rate is calculated using the generator DYMU3 [17]. This calculation is based on structure functions with exponentiation of all leading logarithms including also the most important

(a) Energy (GeV)	Data (Raw)	Background (Corrected MC estimate)			Data (Background Subtracted)
		ISR	Non-prompt	Total	
5-7.5	264	24.2±3.6	58.6± 5.7	82.7± 6.7	181±23(±18± 8±12)
7.5-10	193	15.4±2.9	23.2± 3.6	38.6± 4.6	154±16(±15± 5± 5)
10-15	274	15.8±2.9	15.5± 2.9	31.3± 4.1	243±17(±17± 1± 3)
15-20	173	10.1±2.3	6.0± 1.8	16.1± 3.0	157±14(±14± 3± 2)
20-25	131	2.4±1.1	7.1± 2.0	9.4± 2.3	122±12(±12± 3± 2)
25-30	99	3.2±1.3	7.1± 2.0	10.2± 2.4	89±10(±10± 0± 2)
30-35	72	0.5±0.5	9.8± 2.3	10.3± 2.4	62± 9(± 9± 1± 3)
35-40	73	0.9±0.7	9.3± 2.2	10.2± 2.4	63± 9(± 9± 0± 3)
> 40	57	5.1±1.7	10.4± 2.4	15.4± 2.9	42± 9(± 8± 1± 3)
> 10	879	37.9±4.5	65.1± 6.0	103.0± 7.5	776±37(±31± 9±18)
> 5	1336	77.4±6.5	146.9± 8.9	224.3±11.1	1112±56(±38±22±34)

(b) y_{cut}	Data (Raw)	Background (Corrected MC estimate)			Data (Background Subtracted)
		ISR	Non-prompt	Total	
0.005	1188	70.9±6.2	105.2± 7.6	176.1±9.8	1012±47(±36±17±26)
0.01	1126	63.6±5.9	102.5± 7.5	166.1±9.5	960±46(±35±16±25)
0.02	958	57.4±5.6	73.8± 6.3	131.3±8.5	827±39(±32±12±19)
0.03	844	51.1±5.3	61.6± 5.8	112.7±7.8	731±36(±30±10±16)
0.04	725	45.9±5.0	46.3± 5.0	92.3±7.1	633±31(±28± 6±13)
0.06	569	31.5±4.1	36.0± 4.4	67.4±6.1	502±28(±25± 7±10)
0.08	445	20.5±3.3	32.2± 4.2	52.7±5.4	392±24(±22± 6± 9)
0.1	361	16.6±3.0	31.1± 4.1	47.7±5.1	313±22(±20± 4± 9)
0.15	258	11.0±2.5	33.0± 4.2	44.0±4.9	214±20(±17± 2±10)
0.2	215	7.8±2.1	34.1± 4.3	41.8±4.8	173±19(±15± 2±10)
$y_{cut} = 0.06$ and E_{jet} > 15 GeV	437	26.3±3.8	9.5± 2.3	35.9±4.4	401±22(±21± 4± 3)

Table 1: Number of isolated photon candidates and background fractions as a function of (a) the photon energy and (b) the jet resolution parameter y_{cut} . Errors on the Monte-Carlo predictions are statistical only. The error on the background subtracted data is the total error. The contributions, added in quadrature, for the statistical and the systematic errors coming from the isolation and the background subtraction are given in parentheses.

next-to-leading terms. With this generator, up to two photons are produced in the initial state. Considering that a first order calculation would give 20% more ISR, a conservative systematic uncertainty of 10% is assigned in order to account for possible higher-order terms. The interference between initial and final state radiation is neglected in the vicinity of the Z peak [1].

4.2 Non-Prompt Background

The rate of non-prompt background is calculated using the previously mentioned Monte-Carlo simulation of hadronic events. The hadronisation of quarks and gluons and hadron decays are simulated using JETSET 7.3. The predicted non-prompt background for $E_\gamma > 5$ GeV is 92.6 ± 7.1 events. This background comes mainly from π^0 (70%), η (8%) and long-lived neutral hadrons (12%). The simulation also indicates that 70% of these hadrons come from direct fragmentation. The remaining background is mostly due to ρ decay. Since this background arises from a small part of the particle phase space, its determination is subject to large uncertainties and the following checks have been performed.

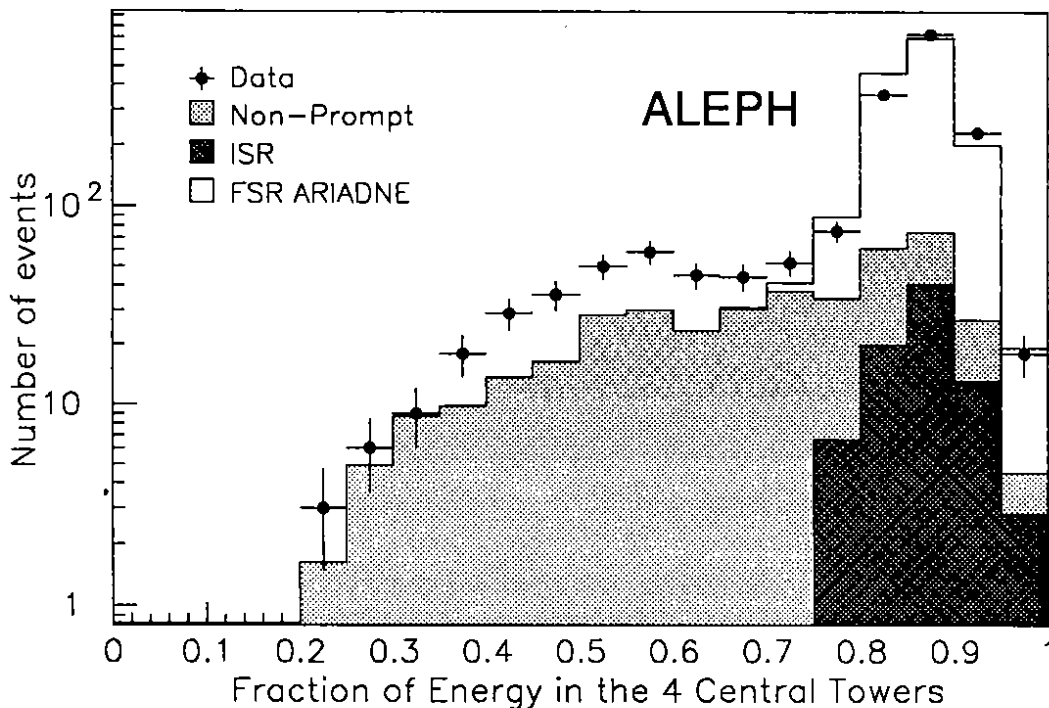


Figure 3: The F_4 distribution of isolated photon candidates satisfying all cuts except the RF_4 cut for photon identification.

A check can be made using candidate ECAL clusters failing the photon identification cut $RF_4 > -2$. The F_4 distribution of candidate clusters satisfying all cuts but leaving out the photon identification cut is shown in figure 3. Isolated photon candidates are concentrated at high values of F_4 . The region $F_4 < 0.75$ is dominated by the non-prompt contribution and can be used as a background monitor. The energy distribution of isolated clusters with $F_4 < 0.75$ is shown in figure 4a. The data show an excess compared with the prediction for $E_\gamma < 15$ GeV.

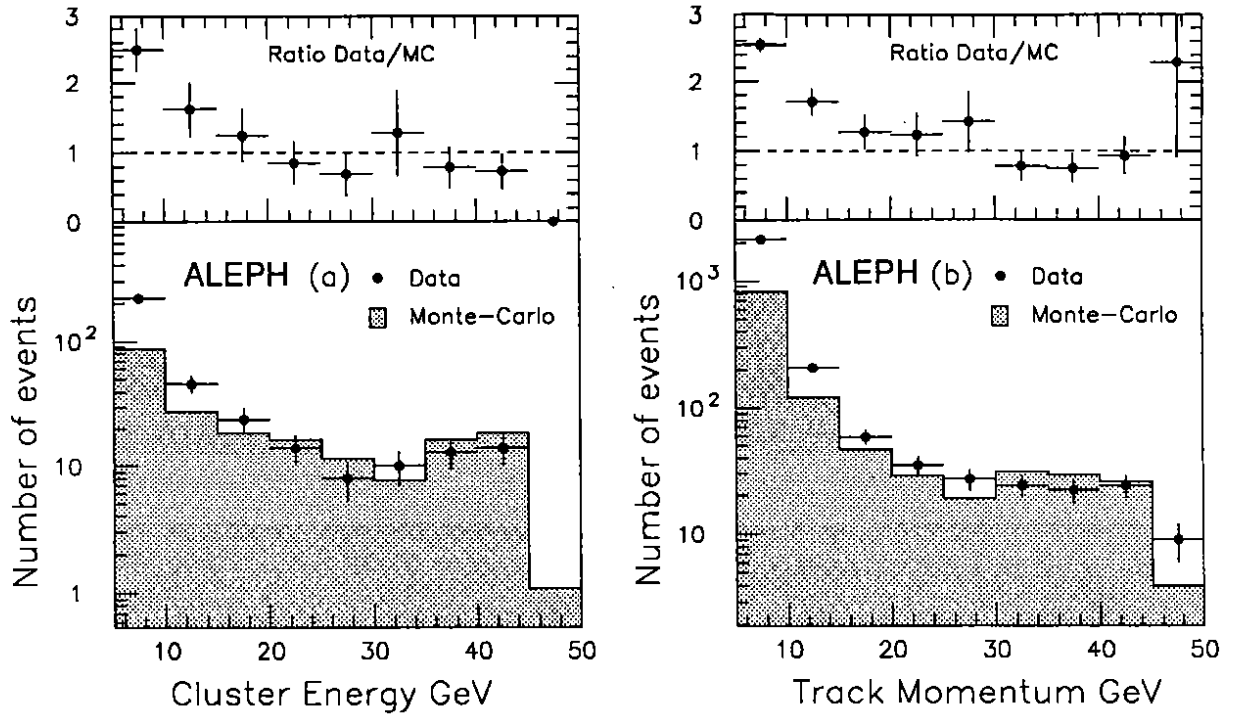


Figure 4: (a) Energy distribution of isolated clusters with $F_4 < 0.75$. (b) Momentum distribution of isolated charged tracks. The ratio of the data to the Monte-Carlo prediction is shown above each distribution.

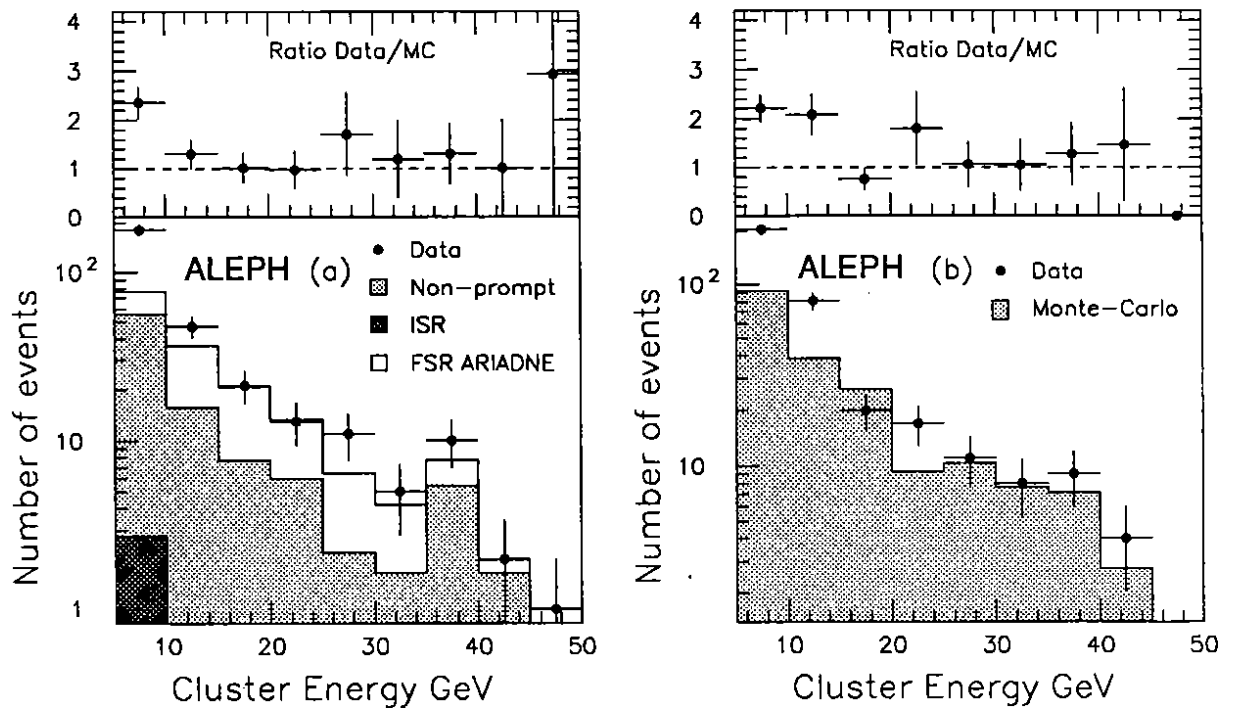


Figure 5: (a) Energy distribution of "tagged" clusters identified as photons ($RF_4 > -2$). (b) Energy distribution of "tagged" clusters with $F_4 < 0.75$. The ratio of the data to the Monte-Carlo prediction is shown above each distribution.

A second check can be made with charged particles using the same isolation and θ_{jet} cuts as for the photon candidates. The momentum distribution of isolated charged tracks is shown in figure 4b. The data show an excess compared with the Monte-Carlo prediction for $p < 15$ GeV while there is acceptable agreement for $p > 15$ GeV.

Another background dominated sample can be defined using candidate clusters having at least one other electromagnetic ECAL cluster with more than 500 MeV in the 20° cone, revealing the presence of a fragmentation halo or decay partners. The energy distribution of this “tagged” sample is shown in figure 5a for photon candidates ($RF_4 > -2$) and in figure 5b for non-photon candidates with $F_4 < 0.75$. The comparison with the Monte-Carlo prediction again reveals an excess of clusters in the data for $E_\gamma < 15$ GeV. This sample also gives some confidence that what is observed for $F_4 < 0.75$ can be extrapolated to the signal region $RF_4 > -2$.

These three checks agree within statistics, indicating an underestimate of the non-prompt background in the simulation. The predicted non-prompt background events are therefore weighted by a factor of 2.5 if $E_\gamma < 10$ GeV and by a factor of 1.5 if $10 < E_\gamma < 15$ GeV. The non-prompt background for $E_\gamma > 5$ GeV then becomes 146.9 ± 8.9 events corresponding to a 11.0% fraction. It is more important at low energy (18% for $E_\gamma < 10$ GeV) and at high energy (15% for $E_\gamma > 30$ GeV) where the separation between photons and π^0 s is less efficient. Although the background rises steeply below 10 GeV, the low energy region between 5 and 10 GeV is included since here the models might diverge substantially in their predictions [2]. As a function of y_{cut} , the non-prompt background decreases from 8.9% for $y_{cut} = 0.005$ to 6.3% for $y_{cut} = 0.06$, then increases to 16% at the highest y_{cut} .

The three checks have a statistical accuracy of about 10% for $E_\gamma < 15$ GeV and 15% for $E_\gamma > 15$ GeV. Extrapolating these observed backgrounds to the signal region, a systematic uncertainty of 20% (30%) is assigned for $E_\gamma < 15$ GeV ($E_\gamma > 15$ GeV). This error translates to a 3% systematic error on the FSR prompt photon rate for $E_\gamma > 5$ GeV.

4.3 FSR Signal and Summary of Systematic Errors

The numbers of prompt photons after background subtraction are given in table 1. The background from $\tau\tau$ and $\gamma\gamma$ events is neglected. Systematic errors on the number of prompt photons with $E_\gamma > 5$ GeV are summarized in table 2.

The total systematic error for the full sample with $E_\gamma > 5$ GeV is 4%, with the main contributions coming from the isolation (2.0%) and the non-prompt background subtraction (3.1%). The number of prompt photons with $E_\gamma > 5$ GeV is

$$1112 \pm 38(stat.) \pm 45(syst.)$$

with a total experimental error of 5.2%.

The systematic errors for $y_{cut} = 0.005$, 0.06 and 0.2 are also indicated in table 2. The error coming from the isolation decreases with increasing y_{cut} as photons are more isolated for larger y_{cut} . The error from the background subtraction decreases down to a minimum of 2% for $y_{cut} = 0.06$ and then increases up to 6% for $y_{cut} = 0.2$.

In the following, only the two main systematic errors (isolation and non-prompt background subtraction) are considered for the estimate of the total systematic error. Their

Error Source	No y_{cut}	$y_{cut} = 0.005$	$y_{cut} = 0.06$	$y_{cut} = 0.2$	$y_{cut} = 0.06$ and $E_{jet} > 15$ GeV
ECAL Energy Calibration	1.0	1.0	1.0	1.0	1.0
Photon Identification	1.0	1.0	1.0	1.0	1.0
Isolation	2.0	1.7	1.4	1.1	1.0
Simulation of jets	0.5	0.5	0.5	0.5	0.5
ISR background	0.6	0.6	0.5	0.4	0.6
Non-prompt background	3.1	2.5	2.0	5.8	0.7
Total systematic error	4.0	3.4	2.9	6.1	2.0
Statistical error	3.4	3.5	4.9	8.9	5.3
Total experimental error	5.2	4.9	5.7	11.	5.7

Table 2: Summary of experimental errors (in %) on the number of prompt photons with $E_\gamma > 5$ GeV. Errors are added in quadrature.

values are indicated in table 1. The error coming from the non-prompt background subtraction is larger than the error coming from the isolation correction except for $15 < E_\gamma < 25$ GeV where the non-prompt background is small. The total systematic error is always comparable or significantly smaller than the statistical error.

This FSR signal can be compared with the predictions of the parton shower models JETSET, ARIADNE and HERWIG.

5 Final State Photon Radiation in Parton Shower Models

5.1 The Parton Shower Models

The parton shower models provide a simulation of the parton cascade based on a leading-logarithm approximation (LLA) of perturbative QCD. The hadronisation process is simulated using a phenomenological approach.

In JETSET [7], coloured partons radiate quarks and gluons according to the QCD splitting functions using a running strong coupling as a function of transverse momentum squared. Soft gluon coherence is taken into account by ordering the emission angles. In addition, the probability of the first branching is matched to the $O(\alpha_s)$ matrix element. The hadronisation of coloured partons is modelled according to the ‘‘Lund string model’’.

Apart from the standard version, three alternative versions of JETSET, studied in [11], are also considered in this paper. The first variant has no matching to the $O(\alpha_s)$ matrix element at the first branching (‘‘No $O(\alpha_s)$ matching’’¹), the second variant has no ordering of the emission angles (‘‘Incoherent’’) and the third variant has a constant $\alpha_s = 0.215$ instead of a running coupling constant (‘‘Constant α_s ’’).

In ARIADNE [8], the parton cascade is formulated in terms of colour dipoles, each dipole radiating according to the $O(\alpha_s)$ matrix element. Soft gluon coherence is included

¹This variant was called ‘‘Without $O(\alpha_s)$ ’’ in [11].

as a consequence of the ordering of the transverse momenta of subsequently radiating dipoles. The hadronisation in ARIADNE is performed as in JETSET.

In HERWIG [9], the parton shower is formulated as in JETSET in terms of QCD splitting functions but with a choice of kinematical variables ensuring gluon coherence and azimuthal correlations within and between jets. Previous versions had shown a depletion in the region of phase space where a hard photon or gluon recoils against a nearly collinear quark-antiquark pair. Version 5.4 includes a correction for this using the $O(\alpha_s)$ matrix element [18]. The hadronisation is done using the “cluster fragmentation” algorithm where no explicit fragmentation functions are used.

The parameters used for JETSET, ARIADNE and HERWIG are given in table 3a. With these parameters, the three generators give a good description of event shape variables and inclusive charged particle distributions in hadronic events [11]. The parameters of the three variants of JETSET, given in table 3b, have also been adjusted to the ALEPH data [11]. With the fitted parameters, the “No $O(\alpha_s)$ matching” variant is almost as good as the standard version whereas the “Constant α_s ” variant and especially the “Incoherent” variant give worse descriptions of the data than the standard version.

In the parton shower models, photon radiation is treated in the same way as gluon radiation, replacing colour charges by electric charges and the QCD running coupling α_s by a fixed electromagnetic coupling taken at the Thomson limit $\alpha = 1/137$ [19]. A separate cut-off parameter is also added for limiting the photon radiation independently of the gluon radiation (M_{min}^γ for JETSET, $p_t^{\gamma,min}$ for ARIADNE and VPCUT for HERWIG).

For each generator, FSR events corresponding to more than 2 million hadronic events were produced and processed through the full ALEPH simulation and reconstruction programs.

5.2 Comparison of the Parton Shower Models with the FSR Signal

The predictions of the parton shower models for the expected number of FSR photons are compared with the data in table 4 as a function of y_{cut} , in figure 6 for the full sample and in figure 7 for the samples with $y_{cut} = 0.005, 0.06$ and 0.2 . The transverse energy (figure 6b) which together with the energy describes the emission process is calculated with respect to the thrust axis. In order to represent the primary event direction, the thrust axis is computed using all energy flow objects in the event, including the photon².

The predicted shapes reproduce the measured shapes of distributions, indicating that final state radiation is indeed responsible for most of the observed events. In the following, it is assumed that the observed events are coming from FSR only. However, some differences between the predictions of JETSET, ARIADNE and HERWIG arise.

The rate predicted by JETSET (see table 4) is too low by (21 ± 6) % compared with the data, confirming the previous measurement by ALEPH [12] and the other LEP collaborations [2]. The excess of data is located at low photon energy. The agreement with the data is therefore better at high y_{cut} where only high energy photons contribute (see figure 7). The excess of data compared with JETSET is located at small transverse energy p_\perp with respect to the thrust axis, at small θ_{jet} and at large E_{jet} .

²The definition of the thrust axis has changed compared with the previous publication [12] where the thrust axis was computed using only charged tracks.

(a)	JETSET 7.3	ARIADNE 4.2	HERWIG 5.4
Strong Coupling	$\Lambda_{LLA} = 310 \text{ MeV}$	$\Lambda_{QCD} = 212 \text{ MeV}$	$\Lambda_{LLA} = 154 \text{ MeV}$
Gluon Radiation	$M_{min}^g = 1.5 \text{ GeV}$	$p_t^{g,min} = 0.90 \text{ GeV}$	$M_g = 0.865 \text{ GeV}$
Photon Radiation	$M_{min}^\gamma = 1 \text{ GeV}$	$p_t^{\gamma,min} = 1 \text{ GeV}$	VPCUT = 1 GeV
Fragmentation Parameters	$\sigma = 0.358 \text{ GeV}$ B = 0.84 GeV ⁻² A = 0.5	$\sigma = 0.364 \text{ GeV}$ B = 0.76 GeV ⁻² A = 0.5	$M_{cl} = 3.65 \text{ GeV}$ VQCUT = 0.48 GeV VGCUT = 0.

(b)	“No $O(\alpha_s)$ matching”	“Incoherent”	“Constant α_s ”
Strong Coupling	$\Lambda_{LLA} = 189 \text{ MeV}$	$\Lambda_{LLA} = 380 \text{ MeV}$	$\alpha_s = 0.215$
Gluon Radiation	$M_{min}^g = 1.18 \text{ GeV}$	$M_{min}^g = 1.59 \text{ GeV}$	$M_{min}^g = 1.07 \text{ GeV}$
Photon Radiation	$M_{min}^\gamma = 1 \text{ GeV}$	$M_{min}^\gamma = 1 \text{ GeV}$	$M_{min}^\gamma = 1 \text{ GeV}$
Fragmentation Parameters	$\sigma = 0.392 \text{ GeV}$ B = 0.63 GeV ⁻² A = 0.5	$\sigma = 0.414 \text{ GeV}$ B = 1.23 GeV ⁻² A = 0.5	$\sigma = 0.421 \text{ GeV}$ B = 0.41 GeV ⁻² A = 0.5

Table 3: Parameters of the parton shower models (a) and the JETSET variants (b). The meaning of these parameters is discussed in [11].

y_{cut}	Data	JETSET		ARIADNE		HERWIG	
		FSR	Ratio	FSR	Ratio	FSR	Ratio
no y_{cut}	1112 ± 56	920 ± 13	1.21 ± 0.06	1190 ± 17	0.93 ± 0.05	1163 ± 16	0.96 ± 0.05
0.005	1012 ± 47	840 ± 12	1.21 ± 0.06	1091 ± 16	0.93 ± 0.05	1050 ± 16	0.96 ± 0.05
0.01	960 ± 46	809 ± 12	1.19 ± 0.06	1054 ± 16	0.91 ± 0.05	1010 ± 15	0.95 ± 0.05
0.02	827 ± 39	728 ± 11	1.14 ± 0.06	920 ± 15	0.90 ± 0.05	896 ± 14	0.92 ± 0.05
0.03	731 ± 36	646 ± 11	1.13 ± 0.06	815 ± 14	0.90 ± 0.05	784 ± 14	0.93 ± 0.05
0.04	633 ± 31	571 ± 10	1.11 ± 0.06	726 ± 13	0.87 ± 0.05	695 ± 13	0.91 ± 0.05
0.06	502 ± 28	446 ± 9	1.12 ± 0.07	576 ± 12	0.87 ± 0.05	543 ± 11	0.92 ± 0.05
0.08	392 ± 24	360 ± 8	1.09 ± 0.07	471 ± 10	0.83 ± 0.06	436 ± 10	0.90 ± 0.06
0.1	313 ± 22	295 ± 7	1.06 ± 0.08	390 ± 10	0.80 ± 0.06	350 ± 9	0.89 ± 0.07
0.15	214 ± 20	201 ± 6	1.06 ± 0.10	268 ± 8	0.80 ± 0.08	222 ± 7	0.97 ± 0.09
0.2	173 ± 19	61 ± 5	1.08 ± 0.12	222 ± 7	0.78 ± 0.09	179 ± 6	0.97 ± 0.11
$y_{cut} = 0.06$ and $E_{jet} > 15 \text{ GeV}$	401 ± 22	338 ± 8	1.19 ± 0.07	417 ± 10	0.96 ± 0.06	397 ± 10	1.01 ± 0.06

Table 4: Comparison of the measured FSR signal with the numbers predicted by parton shower models. For each model, the ratio of the data divided by the prediction is also given. The error on the prediction is statistical only. The error on the ratios corresponds to the quadratic sum of statistical and experimental systematic errors.

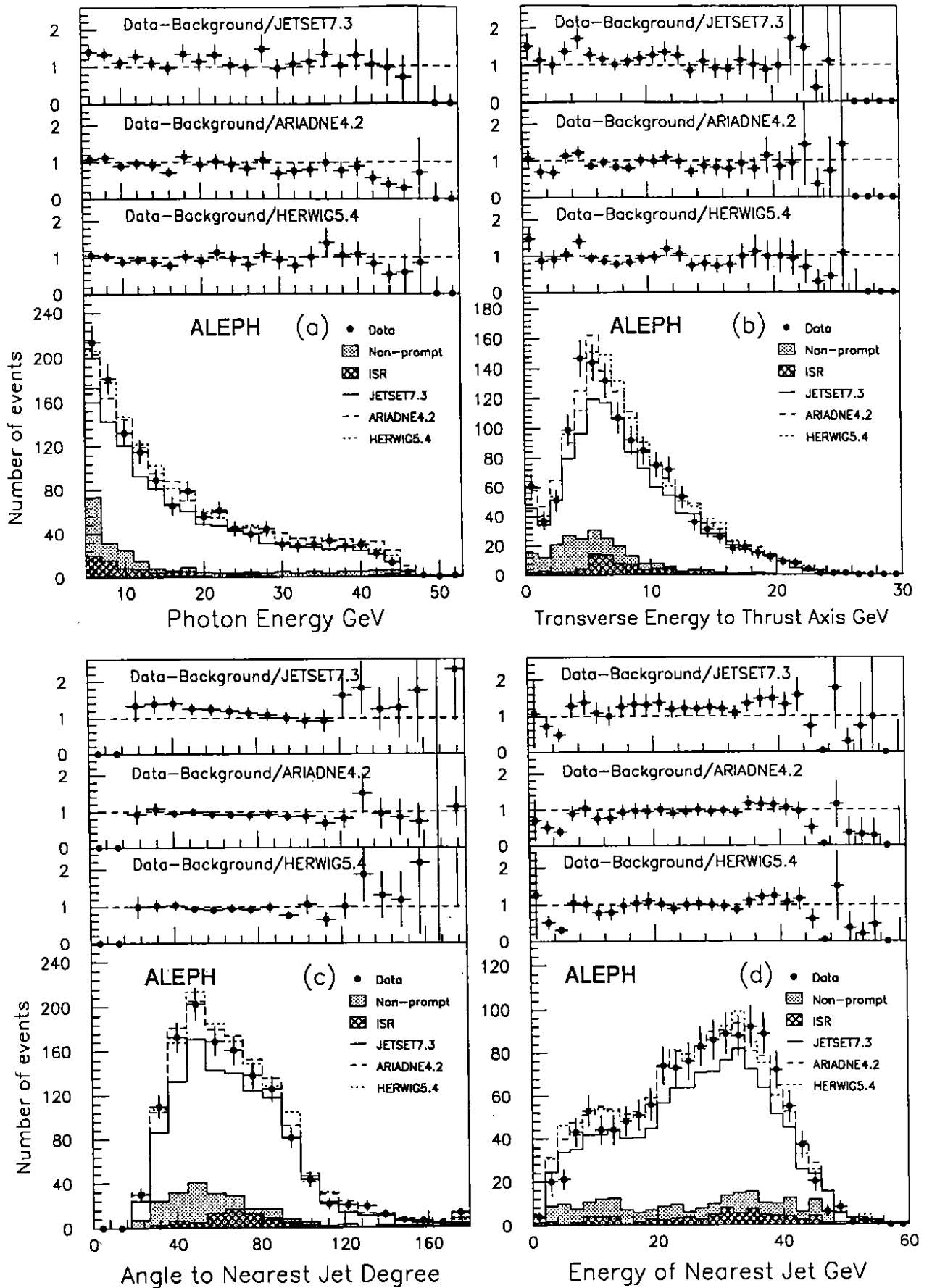


Figure 6: Various distributions of isolated photon candidates (before background subtraction) : (a) energy distribution, (b) transverse energy to thrust axis, (c) angle to the nearest jet and (d) energy of nearest jet. Ratios of the background subtracted data to JETSET, ARIADNE and HERWIG predictions are shown above. Errors are statistical only.

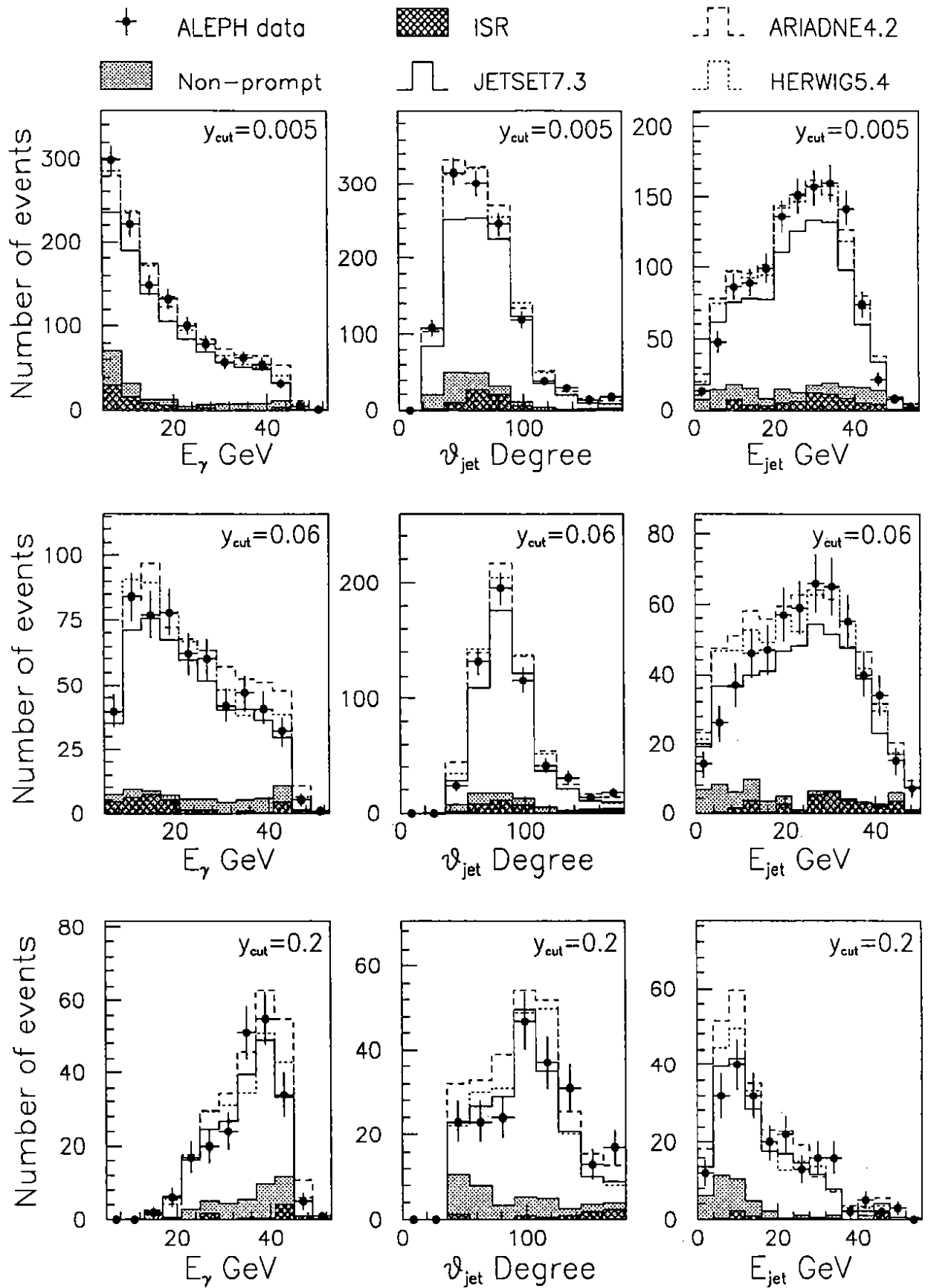


Figure 7: Photon energy, angle to the nearest jet and nearest jet energy distributions for the candidate samples with $y_{cut} = 0.005, 0.06$ and 0.2 . The data are compared with the predictions of parton shower models. Errors are statistical only.

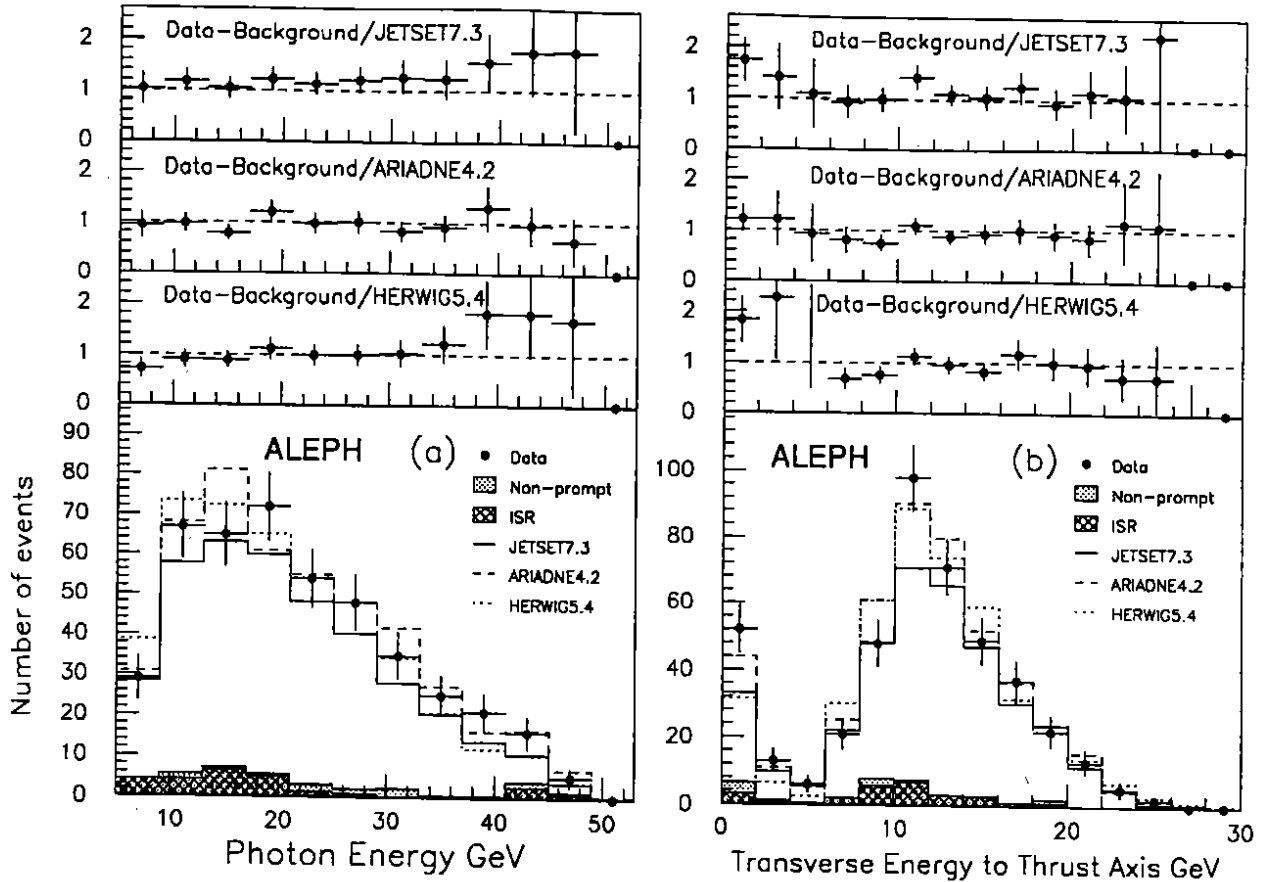


Figure 8: Energy distribution (a) and transverse energy to thrust axis (b) of isolated photon candidates with $y_{cut} = 0.06$ and $E_{jet} > 15$ GeV. Ratios of the background subtracted data to JETSET, ARIADNE and HERWIG predictions are shown above.

Figure 7 indicates that the non-prompt background is reduced for $E_{jet} > 15$ GeV at higher values of y_{cut} . In the sample with $y_{cut} = 0.06$ and $E_{jet} > 15$ GeV, only 2.2% remains, inducing a small systematic error of 0.5% on the FSR signal (table 2). Comparing this clean signal with the predictions of the parton shower models (table 4), the excess of data with respect to JETSET remains. A miscalculation of the non-prompt background is therefore excluded as an explanation for the discrepancy between the data and JETSET.

The rate predicted by ARIADNE is slightly higher than the data (table 4). This tendency is more pronounced for large values of y_{cut} . This can be related to the fact that for the energy distribution (figure 6a) the ARIADNE prediction agrees well with the data at low photon energy but is too high at high photon energy. On the other hand, the shape of the p_{\perp} distribution (figure 6b) is reproduced well by ARIADNE. The HERWIG predictions are similar to those provided by ARIADNE with rather better agreement over the full y_{cut} range (table 4).

Final conclusions are drawn after the theoretical errors on the parton shower model predictions have been evaluated.

6 Determination of the Final State Photon Production Rate

To compare the measurements with other experiments and with theoretical estimates at parton level, the observed numbers of events are corrected for detector and hadronisation effects.

6.1 Acceptance Corrections

Acceptance correction factors are computed using the parton shower models described previously. The acceptance factor is defined as the observed number of events divided by the corresponding number of FSR events generated at the parton level.

At parton level, it is required that $E_\gamma > 5$ GeV, $|\cos \theta_\gamma| < 0.95$ and that the energy sum of all partons inside a 20° cone around the photon is less than 500 MeV. With these cuts, the FSR rate is expressed in a region close to the experimentally accessible region, therefore reducing extrapolations into unmeasurable domains of phase space where the theoretical error could be large. Furthermore, these cuts are useful to get reliable predictions in matrix element calculations [4].

The acceptance correction factor as a function of y_{cut} is shown in figure 9 for JETSET, ARIADNE and HERWIG separately. The factors vary between 58% for $y_{cut} = 0.005$ to 72% for $y_{cut} = 0.2$. The inefficiency at high y_{cut} is mainly due to geometrical effects (conversions in front of the ECAL, coverage and cracks of the ECAL, photon identification cuts) while the reduction of efficiency at low y_{cut} is due both to the isolation condition and the cut on transverse energy at 5 GeV with respect to the beam axis. Some disagreements at the level of 5% are observed. The HERWIG acceptance has a tendency to be systematically lower than those from JETSET and ARIADNE. If the acceptance correction factors are considered separately for each jet multiplicity, discrepancies of up to 15% are seen for $y_{cut} = 0.005$ for the $\gamma + 2$ jets rate.

The acceptance factor is shown in figure 10 as a function of the photon energy (a) and the photon transverse energy with respect to the thrust axis (b) for $y_{cut} = 0.005$ and $y_{cut} = 0.06$. The maximum difference between the values given by the parton shower models is 10% for $y_{cut} = 0.005$ (figure 10a) and 10% for $p_\perp < 2.5$ GeV (figure 10b). For $y_{cut} = 0.06$, no clear systematic trend is visible ; the acceptance factors agree within errors.

The acceptance factors from JETSET, ARIADNE and HERWIG are averaged, weighting each value by the inverse of its statistical error squared. A theoretical error of 5% is assigned to the acceptance factor. When the maximum difference between the average value and any of the three individual values is larger than 5%, this maximum difference is taken as the theoretical error. The theoretical error is added quadratically to the statistical error. Average acceptance correction factors are given in table 5 as a function of y_{cut} . Variations of the acceptance correction factors due to a change of one of the parton shower parameters (table 3) are smaller than 5%. The qualitative conclusions of the paper do not change if for the comparison with a given parton shower model the acceptance as determined by this model is used instead of the average.

The corrected FSR rate as a function of y_{cut} is given in table 5. The relative theoretical error coming from the acceptance correction is comparable to the experimental error at $y_{cut} = 0.005$ and decreases as y_{cut} increases.

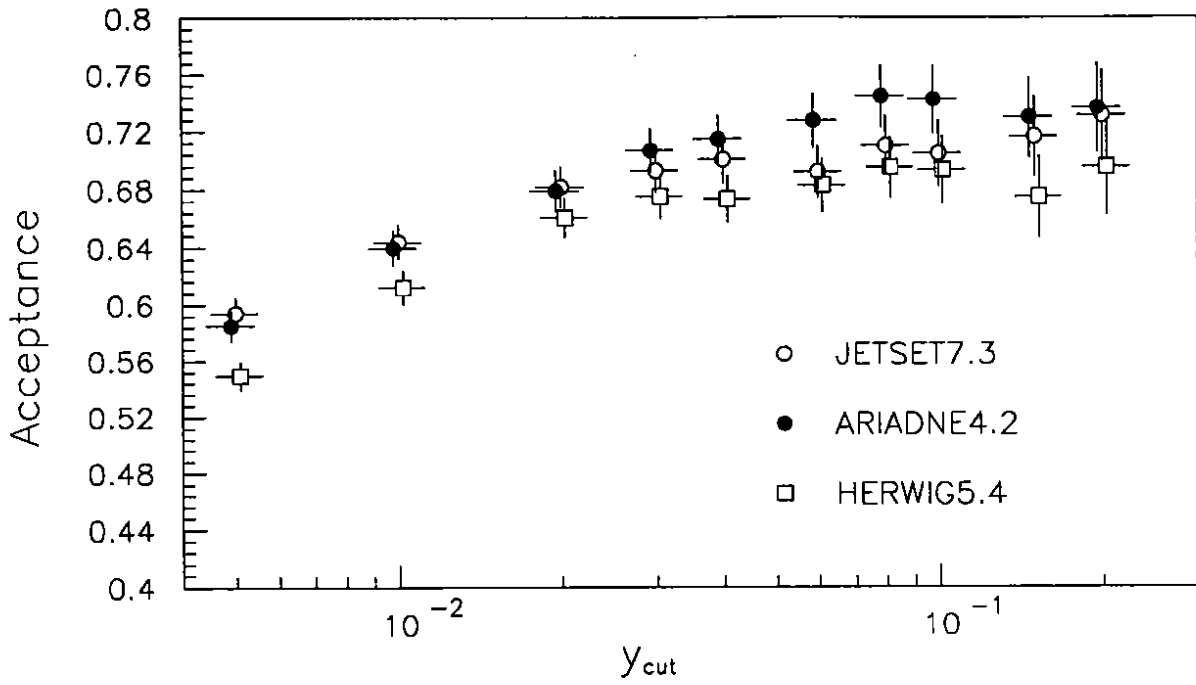


Figure 9: Acceptance correction factor as a function of y_{cut} computed with JETSET, ARIADNE and HERWIG. Errors are statistical only.

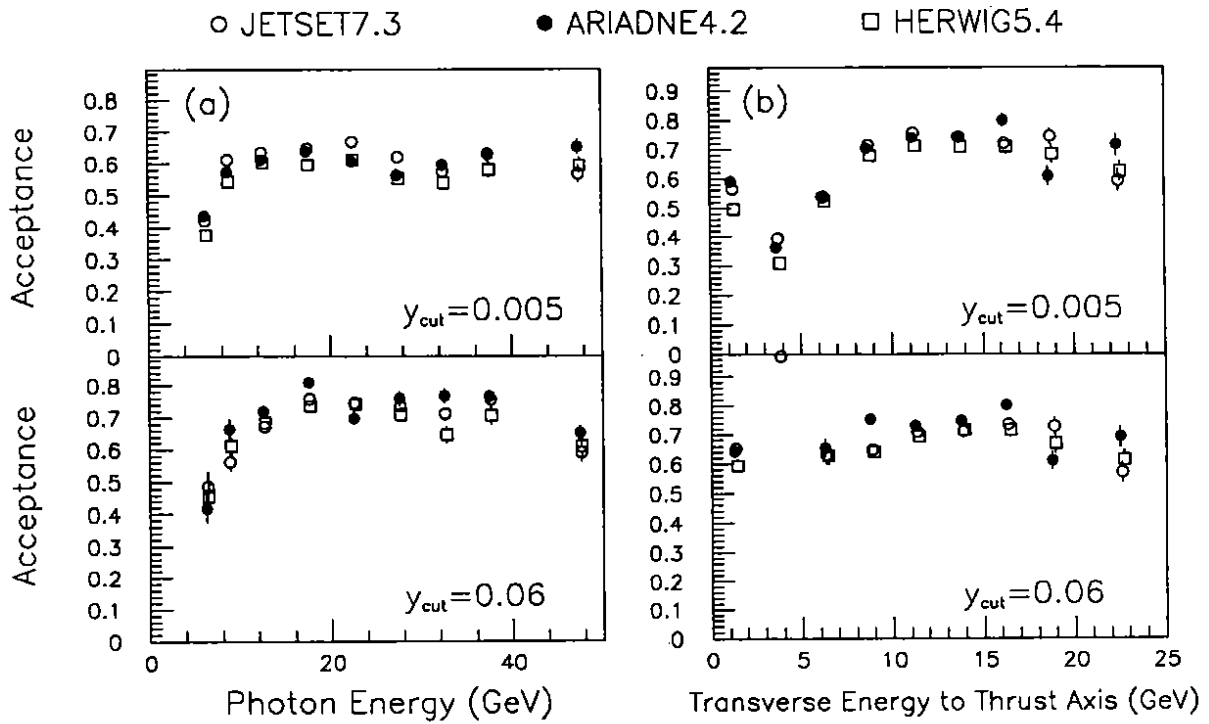


Figure 10: Acceptance correction factor for $y_{cut} = 0.005$ and 0.06 as a function of (a) photon energy and (b) photon transverse energy with respect to the thrust axis. Errors are statistical only.

y_{cut}	Acceptance	FSR rate
0.005	0.575 ± 0.029	$3.82 \pm 0.26(\pm 0.18 \pm 0.20)$
0.01	0.631 ± 0.032	$3.30 \pm 0.23(\pm 0.16 \pm 0.17)$
0.02	0.674 ± 0.035	$2.67 \pm 0.19(\pm 0.13 \pm 0.14)$
0.03	0.692 ± 0.036	$2.30 \pm 0.16(\pm 0.11 \pm 0.12)$
0.04	0.696 ± 0.036	$1.98 \pm 0.14(\pm 0.10 \pm 0.10)$
0.06	0.700 ± 0.037	$1.56 \pm 0.12(\pm 0.09 \pm 0.08)$
0.08	0.716 ± 0.038	$1.19 \pm 0.10(\pm 0.07 \pm 0.06)$
0.1	0.713 ± 0.038	$0.95 \pm 0.08(\pm 0.07 \pm 0.05)$
0.15	0.707 ± 0.039	$0.66 \pm 0.07(\pm 0.06 \pm 0.04)$
0.20	0.721 ± 0.041	$0.52 \pm 0.06(\pm 0.06 \pm 0.03)$

Table 5: Acceptance corrections and FSR event rate per 1000 hadronic events as a function of y_{cut} . The error on the acceptance includes the estimate of the theoretical error. The error on the FSR rate is the total error. The errors in parentheses are the experimental error and the theoretical error from the acceptance correction respectively.

y_{cut}	$\gamma + 1$ jet	$\gamma + 2$ jets	$\gamma + \geq 3$ jets
0.005	$0.01 \pm 0.01(\pm 0.01 \pm 0.00)$	$1.11 \pm 0.21(\pm 0.08 \pm 0.19)$	$2.73 \pm 0.20(\pm 0.14 \pm 0.14)$
0.01	$0.03 \pm 0.03(\pm 0.01 \pm 0.02)$	$1.57 \pm 0.16(\pm 0.10 \pm 0.13)$	$1.72 \pm 0.13(\pm 0.10 \pm 0.09)$
0.02	$0.04 \pm 0.01(\pm 0.01 \pm 0.01)$	$1.96 \pm 0.14(\pm 0.10 \pm 0.10)$	$0.66 \pm 0.07(\pm 0.06 \pm 0.04)$
0.03	$0.04 \pm 0.02(\pm 0.02 \pm 0.01)$	$1.92 \pm 0.14(\pm 0.09 \pm 0.10)$	$0.33 \pm 0.05(\pm 0.04 \pm 0.02)$
0.04	$0.05 \pm 0.02(\pm 0.02 \pm 0.01)$	$1.75 \pm 0.13(\pm 0.09 \pm 0.09)$	$0.17 \pm 0.03(\pm 0.03 \pm 0.01)$
0.06	$0.10 \pm 0.03(\pm 0.02 \pm 0.01)$	$1.41 \pm 0.11(\pm 0.08 \pm 0.07)$	$0.05 \pm 0.02(\pm 0.02 \pm 0.01)$
0.08	$0.13 \pm 0.03(\pm 0.03 \pm 0.01)$	$1.05 \pm 0.09(\pm 0.06 \pm 0.06)$	$0.01 \pm 0.01(\pm 0.01 \pm 0.00)$
0.10	$0.17 \pm 0.03(\pm 0.03 \pm 0.01)$	$0.79 \pm 0.07(\pm 0.05 \pm 0.04)$	$0.00 \pm 0.00(\pm 0.00 \pm 0.00)$
0.15	$0.26 \pm 0.04(\pm 0.04 \pm 0.02)$	$0.40 \pm 0.05(\pm 0.04 \pm 0.02)$	$0.00 \pm 0.00(\pm 0.00 \pm 0.00)$
0.20	$0.36 \pm 0.05(\pm 0.05 \pm 0.02)$	$0.16 \pm 0.03(\pm 0.03 \pm 0.01)$	$0.00 \pm 0.00(\pm 0.00 \pm 0.00)$

Table 6: The corrected $\gamma + n$ jet rates per 1000 hadronic events as a function of y_{cut} . The error on each FSR rate is the total error. The errors in parentheses are the experimental error and the theoretical error from the acceptance correction respectively.

Energy (GeV)	$y_{cut} = 0.005$	$y_{cut} = 0.06$	$y_{cut} = 0.2$
5-7.5	$289 \pm 43 (\pm 35 \pm 25)$	$28.2 \pm 9.0 (\pm 8.6 \pm 2.6)$	$0.0 \pm 0.0 (\pm 0.0 \pm 0.0)$
7.5-10	$198 \pm 25 (\pm 22 \pm 13)$	$49.8 \pm 10.6 (\pm 9.5 \pm 4.6)$	$0.0 \pm 0.0 (\pm 0.0 \pm 0.0)$
10-15	$161 \pm 14 (\pm 12 \pm 8)$	$64.5 \pm 7.7 (\pm 6.9 \pm 3.4)$	$0.1 \pm 0.6 (\pm 0.6 \pm 0.0)$
15-20	$105 \pm 11 (\pm 10 \pm 5)$	$43.2 \pm 6.0 (\pm 5.5 \pm 2.4)$	$1.4 \pm 2.2 (\pm 1.0 \pm 2.0)$
20-25	$82 \pm 9 (\pm 8 \pm 5)$	$45.1 \pm 6.3 (\pm 5.8 \pm 2.4)$	$10.2 \pm 3.2 (\pm 2.8 \pm 1.4)$
25-30	$64 \pm 9 (\pm 8 \pm 5)$	$38.5 \pm 5.6 (\pm 5.2 \pm 2.0)$	$9.7 \pm 3.1 (\pm 2.8 \pm 1.4)$
30-35	$47 \pm 8 (\pm 7 \pm 3)$	$28.6 \pm 5.4 (\pm 4.6 \pm 2.8)$	$14.2 \pm 3.8 (\pm 3.0 \pm 2.4)$
35-40	$42 \pm 7 (\pm 6 \pm 3)$	$26.2 \pm 4.7 (\pm 4.5 \pm 1.5)$	$40.0 \pm 7.1 (\pm 6.1 \pm 3.7)$
40-55	$10 \pm 2 (\pm 2 \pm 1)$	$9.2 \pm 1.9 (\pm 1.9 \pm 0.5)$	$10.4 \pm 2.4 (\pm 2.1 \pm 1.0)$

Table 7: The differential FSR event rate per 10^6 hadronic events per GeV as a function of the photon energy. The error on each FSR rate is the total error. The errors in parentheses are the experimental error and the theoretical error from the acceptance correction respectively.

p_{\perp} (GeV)	$y_{cut} = 0.005$	$y_{cut} = 0.06$	$y_{cut} = 0.2$
0-2.5	$116 \pm 23 (\pm 20 \pm 12)$	$91.8 \pm 16.6 (\pm 15.5 \pm 5.9)$	$102 \pm 18 (\pm 18 \pm 6)$
2.5-5	$424 \pm 68 (\pm 45 \pm 51)$	$17.5 \pm 5.8 (\pm 4.8 \pm 3.2)$	$33.6 \pm 8.4 (\pm 8.0 \pm 2.3)$
5-7.5	$380 \pm 37 (\pm 31 \pm 20)$	$37.3 \pm 8.7 (\pm 8.4 \pm 8.2)$	$12.9 \pm 4.2 (\pm 4.1 \pm 0.7)$
7.5-10	$235 \pm 23 (\pm 19 \pm 12)$	$88.1 \pm 15.2 (\pm 12.0 \pm 9.3)$	$10.9 \pm 4.1 (\pm 3.4 \pm 2.3)$
10-12.5	$180 \pm 18 (\pm 16 \pm 9)$	$156 \pm 17 (\pm 15 \pm 8)$	$8.9 \pm 9.5 (\pm 3.1 \pm 8.9)$
12.5-15	$101 \pm 13 (\pm 12 \pm 5)$	$99.1 \pm 12.8 (\pm 11.7 \pm 5.2)$	$3.6 \pm 4.2 (\pm 2.2 \pm 3.6)$
15-17.5	$58 \pm 10 (\pm 8 \pm 4)$	$59.9 \pm 9.5 (\pm 8.5 \pm 4.1)$	$3.3 \pm 2.1 (\pm 2.0 \pm 0.6)$
17.5-20	$40 \pm 9 (\pm 8 \pm 5)$	$42.9 \pm 8.9 (\pm 7.8 \pm 4.3)$	$9.9 \pm 3.5 (\pm 3.4 \pm 0.8)$
20-25	$158 \pm 38 (\pm 33 \pm 18)$	$15.6 \pm 3.8 (\pm 3.3 \pm 1.8)$	$15.5 \pm 4.2 (\pm 3.4 \pm 2.4)$

Table 8: The differential FSR event rate per 10^6 hadronic events per GeV as a function of the photon transverse energy with respect to the thrust axis. The error on each FSR rate is the total error. The errors in parentheses are the experimental error and the theoretical error from the acceptance correction respectively.

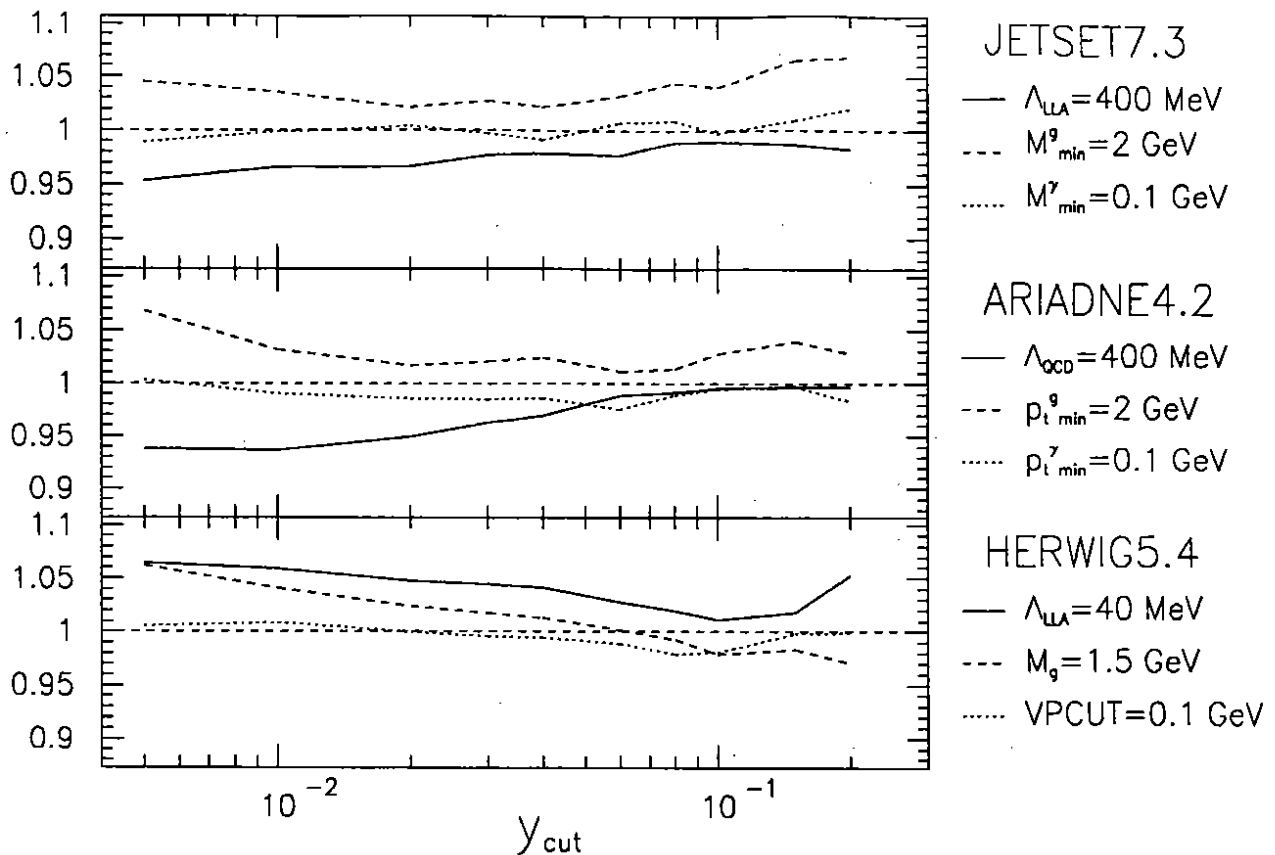


Figure 11: Relative changes to the FSR rate predicted by parton shower models as a function of y_{cut} . One parameter is changed at a time. Each line corresponds to the new value of the parameter indicated on the right hand side while all the other parameters are fixed at their default values given in table 3.

The corrected $\gamma + n$ jet rates are given in table 6. Separate acceptance correction factors are used for each jet multiplicity. The error on the $\gamma + 1$ jet rate is dominated by the experimental error. The error on the $\gamma + 2$ jet rate is dominated by the error from the acceptance correction for $y_{cut} < 0.01$. The experimental error dominates the $\gamma + \geq 3$ jet rate except for small y_{cut} where it is comparable to the error coming from the acceptance correction.

The corrected FSR rates as a function of E_γ and p_\perp are given in tables 7 and 8. The error on the differential FSR rate as a function of the photon energy is dominated by the experimental error. The error on the differential FSR rate as a function of p_\perp is dominated by the experimental error except for $2.5 < p_\perp < 5$ GeV where systematic effects from the acceptance correction seem important.

6.2 Comparison with Parton Shower Models

The FSR rates at parton level predicted by the models are given in table 9 as a function of y_{cut} .

The Monte-Carlo errors on the predictions are obtained in the following way. The parameters controlling the parton cascade were changed, one at a time, to the values given in figure 11 which shows the effects of these changes on the FSR rate as a function of y_{cut} .

y_{cut}	Data	JETSET	ARIADNE	HERWIG
0.005	3.82 ± 0.26	3.08 ± 0.07	4.13 ± 0.07	4.18 ± 0.04
0.01	3.30 ± 0.23	2.73 ± 0.05	3.66 ± 0.04	3.60 ± 0.03
0.02	2.67 ± 0.19	2.29 ± 0.03	3.03 ± 0.03	2.94 ± 0.02
0.03	2.30 ± 0.16	1.99 ± 0.03	2.62 ± 0.03	2.53 ± 0.02
0.04	1.98 ± 0.14	1.75 ± 0.02	2.30 ± 0.02	2.23 ± 0.02
0.06	1.56 ± 0.12	1.36 ± 0.02	1.80 ± 0.02	1.73 ± 0.01
0.08	1.19 ± 0.10	1.06 ± 0.02	1.44 ± 0.02	1.37 ± 0.01
0.1	0.95 ± 0.08	0.86 ± 0.02	1.19 ± 0.02	1.11 ± 0.01
0.15	0.66 ± 0.07	0.56 ± 0.01	0.81 ± 0.01	0.73 ± 0.01
0.2	0.52 ± 0.06	0.44 ± 0.01	0.66 ± 0.01	0.58 ± 0.01

Table 9: Comparison of the acceptance corrected FSR rate per 1000 hadronic events with JETSET, ARIADNE and HERWIG predictions. The error on the data is the total error. The error on each prediction is the total Monte-Carlo error.

The effects due to changing the parameter limiting the photon radiation ($M_{min}^\gamma, p_t^{\gamma,min}$, VPCUT) are negligible provided its value is kept well below the minimum photon energy. The observed changes due to the other two considered parameters (Λ and $M_{min}^g, p_t^{g,min}, M_g$) were then rescaled to correspond to one standard deviation of the fit [11] which determined the values of these parameters. The scaled changes due to Λ and $M_{min}^g, p_t^{g,min}, M_g$ were added quadratically to the statistical error to give the total Monte-Carlo error.

The Monte-Carlo errors to the JETSET, ARIADNE and HERWIG predictions are small and similar. They amount to 2% at $y_{cut} = 0.005$, 1% at $y_{cut} = 0.06$ and 2% at $y_{cut} = 0.2$. The ARIADNE and HERWIG predictions agree within errors at the smallest y_{cut} but are significantly different at higher y_{cut} . The JETSET predictions differ significantly from the ARIADNE and HERWIG predictions at all values of y_{cut} .

The FSR rates predicted by the parton shower models are compared with the data in figures 12 to 18.

The JETSET prediction is three standard deviations too low at low y_{cut} whereas the ARIADNE prediction is two to three standard deviations higher than the data at high values of y_{cut} . The HERWIG prediction is within one to two standard deviations of the data.

In figure 13, the data are compared with the three alternative versions of JETSET. The prediction of the ‘‘Incoherent’’ variant is lower than the prediction of the standard version and hence gives an even worse description of the data. However, the ‘‘No $O(\alpha_s)$ matching’’ and the ‘‘Constant α_s ’’ variants are in good agreement with the data. This is also true in the case of the $\gamma + n$ jet rates where the ‘‘Constant α_s ’’ variant of JETSET provides the best description of data over the full y_{cut} range (figure 14). These conclusions remain if for a comparison with a given model, the acceptance corrections given by this model are used instead of the average.

Comparing the data with the predictions, the various parton shower models or some variants of a given model can be disentangled. This is not easily done by analyzing the

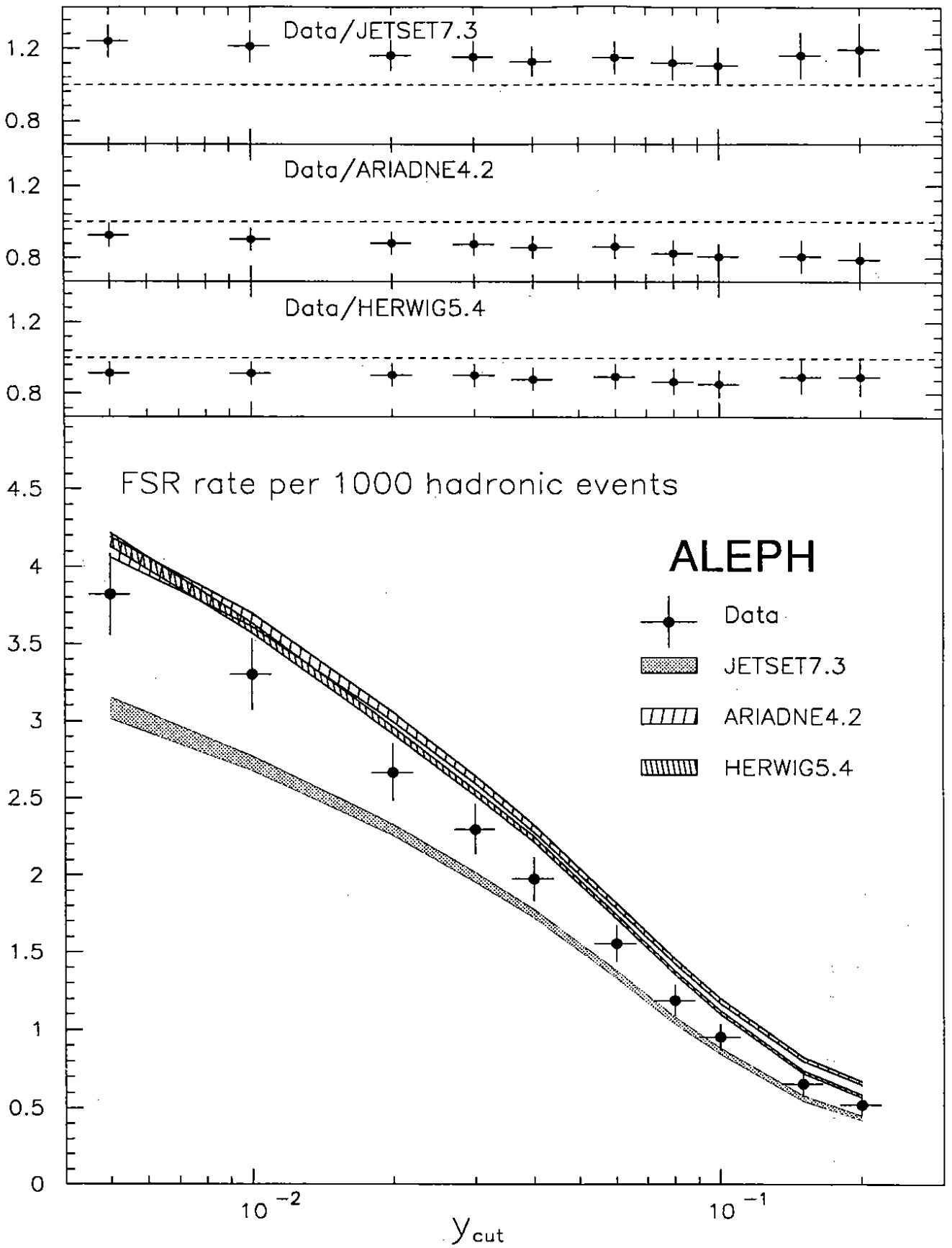


Figure 12: The acceptance corrected FSR rate as a function of y_{cut} and its comparison with parton shower models. The band around each prediction corresponds to the statistical and theoretical errors added in quadrature.

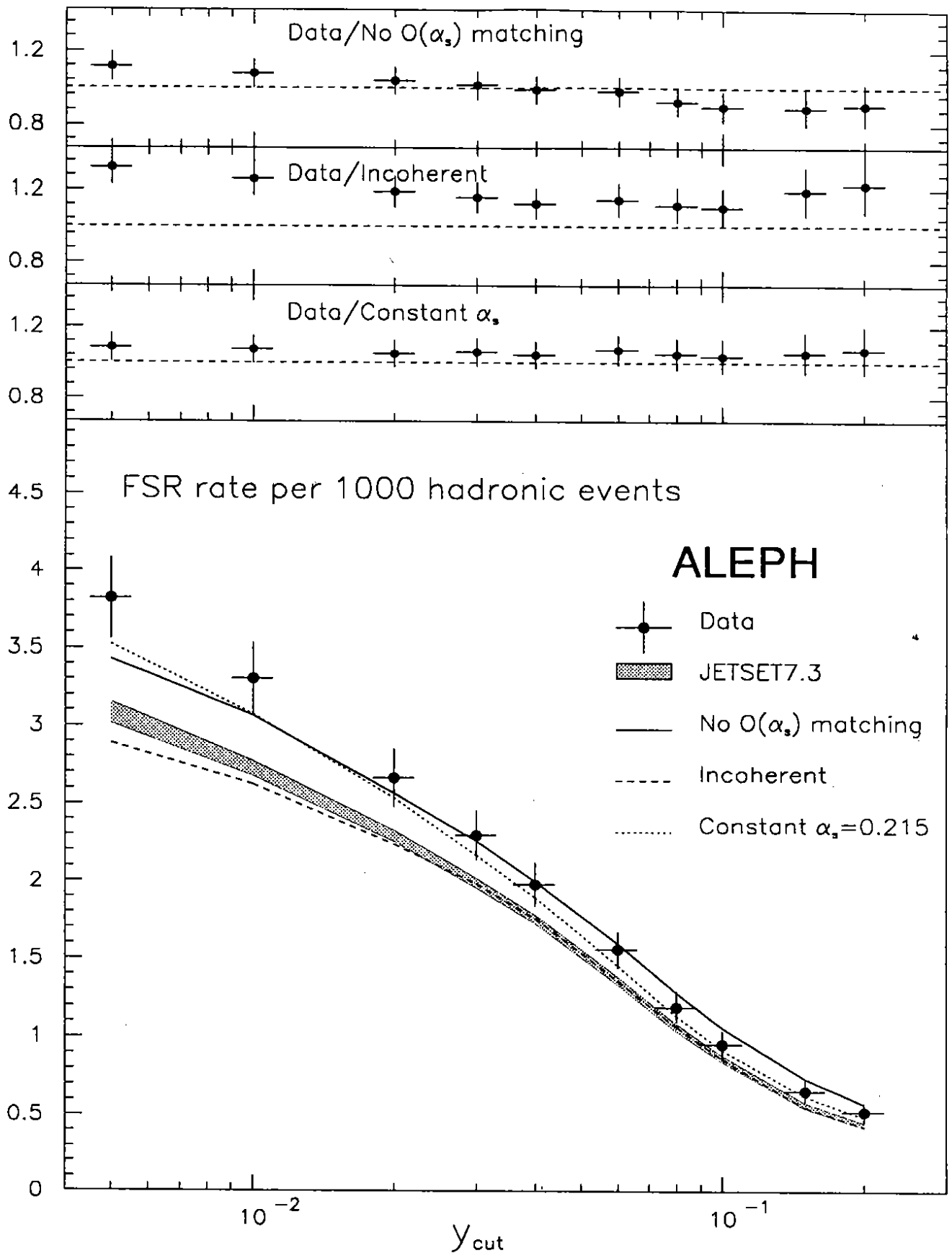


Figure 13: The acceptance corrected FSR rate as a function of y_{cut} and its comparison with the three alternative versions of the JETSET model. The band around the standard JETSET prediction corresponds to the statistical and theoretical errors added in quadrature. A similar band could be drawn around the predictions of the variants.

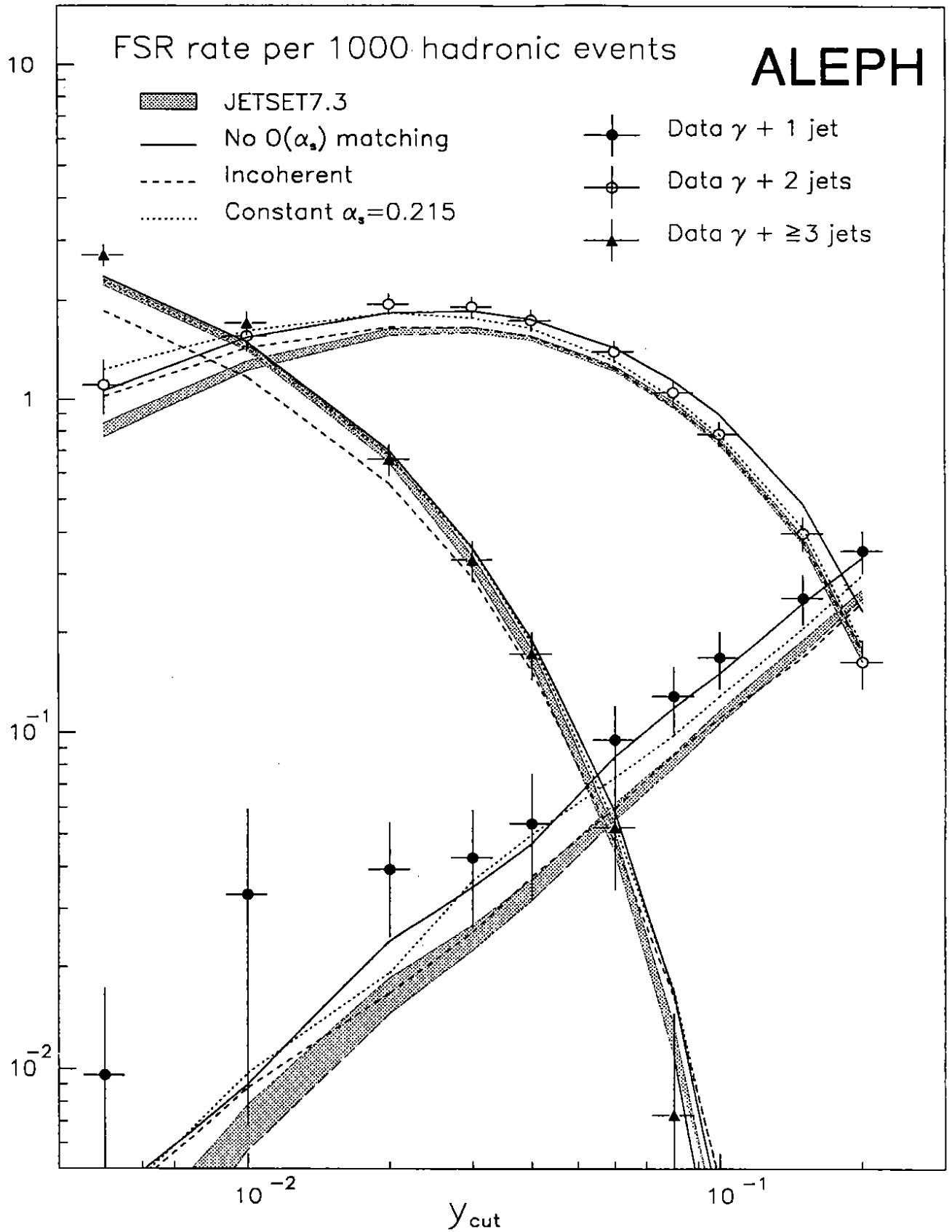


Figure 14: The acceptance corrected $\gamma + n$ jet rates as a function of y_{cut} and their comparison with the JETSET predictions. The predictions of the three variants are also shown. The bands around the JETSET predictions correspond to the statistical and theoretical errors added in quadrature.

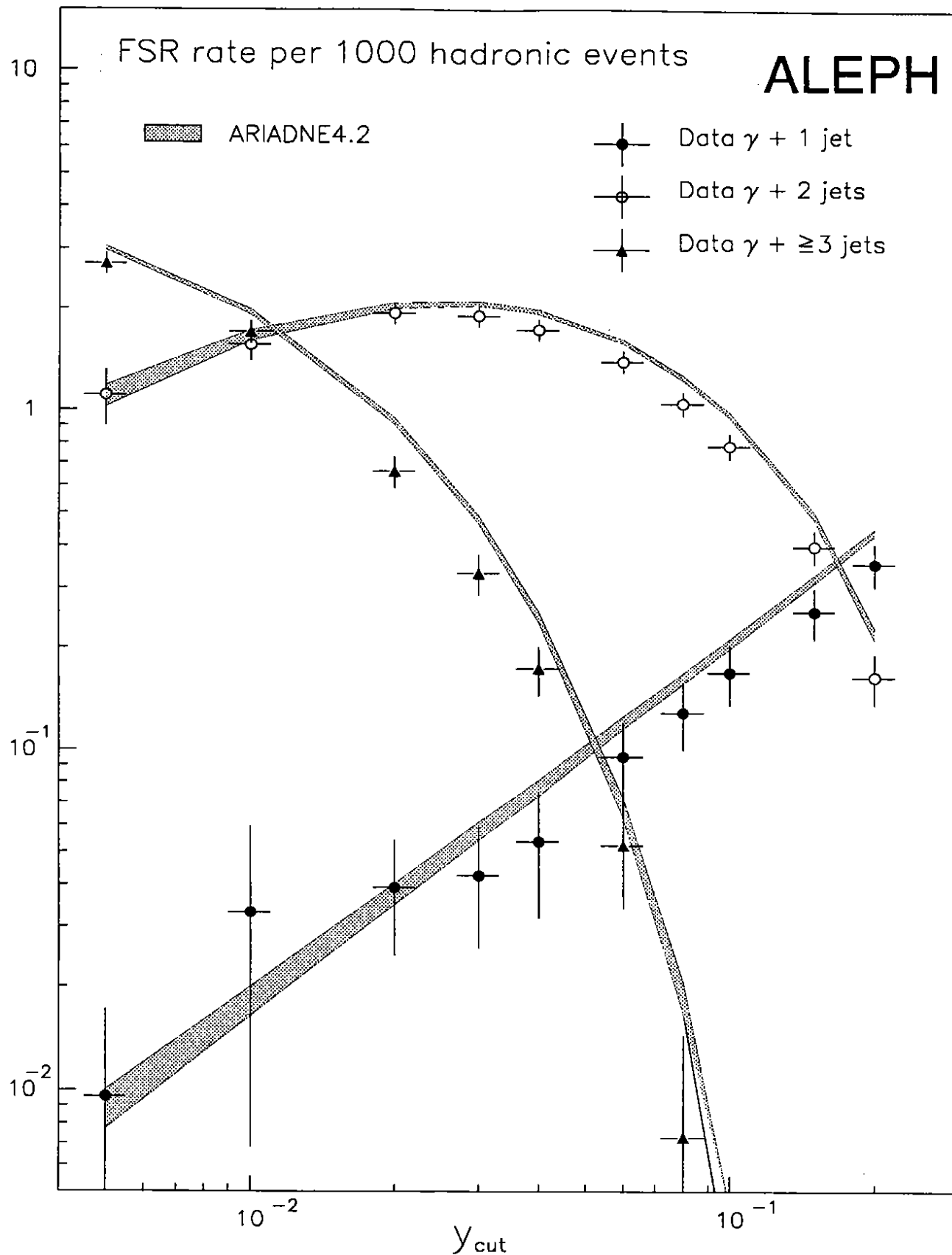


Figure 15: The acceptance corrected $\gamma + n$ jet rates as a function of y_{cut} and their comparison with the ARIADNE predictions. The bands around the predictions correspond to the statistical and theoretical errors added in quadrature.

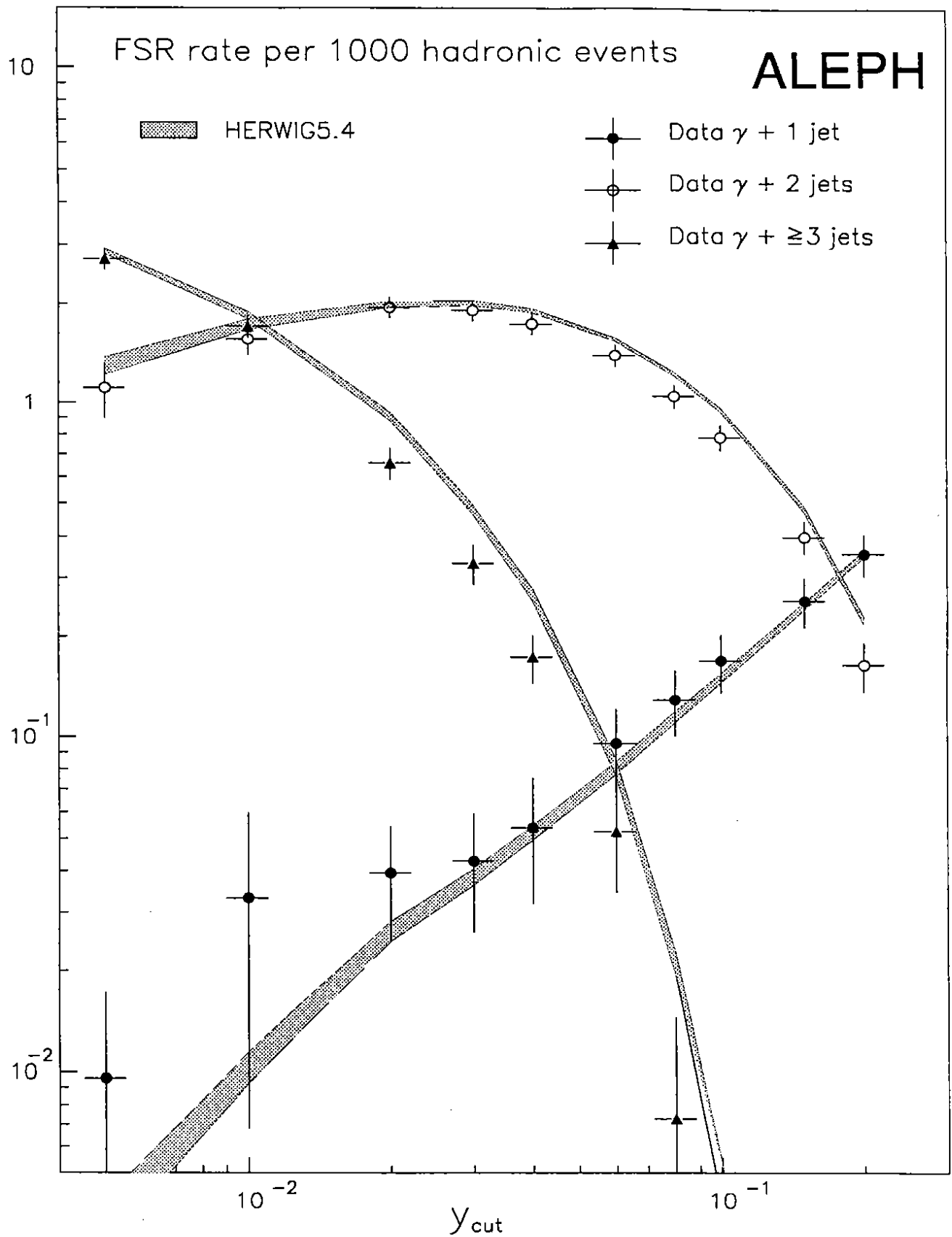



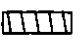


Figure 16: The acceptance corrected $\gamma + n$ jet rates as a function of y_{cut} and their comparison with the HERWIG predictions. The bands around the predictions correspond to the statistical and theoretical errors added in quadrature.

ALEPH  Data  ARIADNE4.2
 JETSET7.3  HERWIG5.4

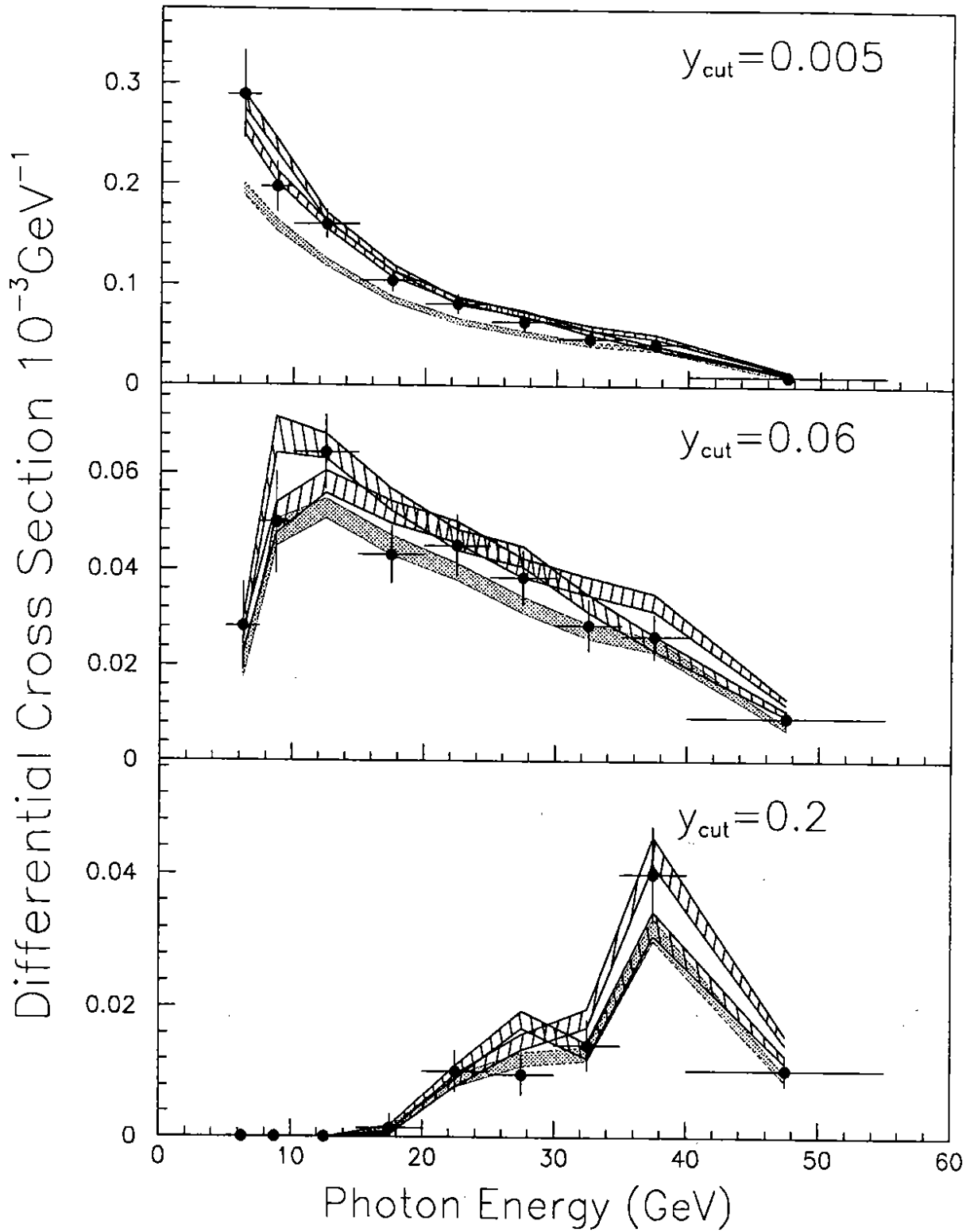


Figure 17: The differential FSR rate as a function of the photon energy and its comparison with parton shower models. The band around each prediction corresponds to the statistical error only.

ALEPH

● Data

▨ ARIADNE4.2

▩ JETSET7.3

▧ HERWIG5.4

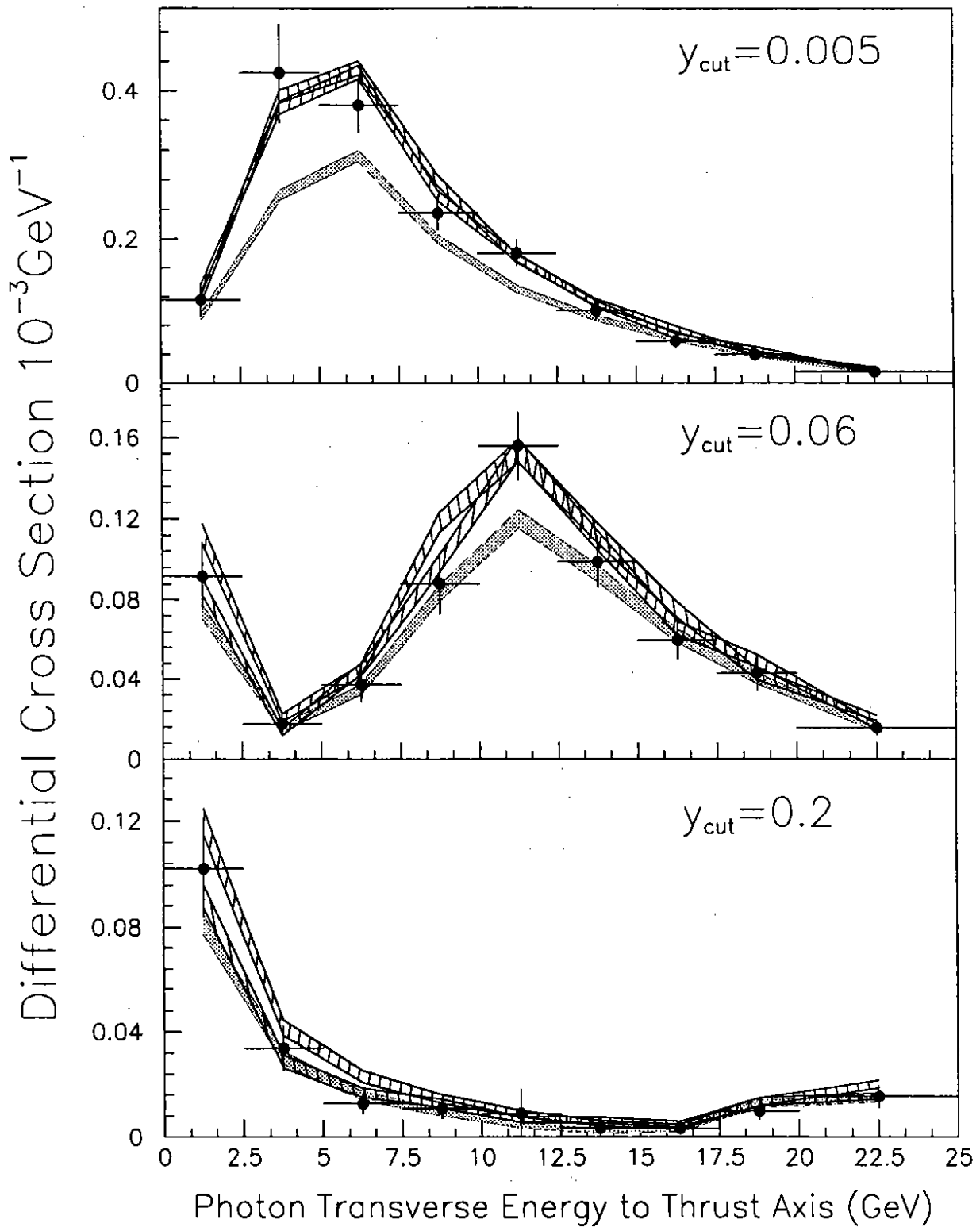


Figure 18: The differential FSR rate as a function of the transverse energy with respect to the thrust axis and its comparison with parton shower models. The band around each prediction corresponds to the statistical error only.

y_{cut}	Data	GNJETS		Glover and Stirling	
		$\alpha_s = 0.118$	$\alpha_s = 0.177$	$\alpha_s = 0.118$	$\alpha_s = 0.103$
0.005	3.82 ± 0.26	4.47 ± 0.36		6.67 ± 0.07	6.56 ± 0.06
0.01	3.30 ± 0.23	4.05 ± 0.16	3.64 ± 0.02	4.95 ± 0.05	4.95 ± 0.04
0.02	2.67 ± 0.19	3.32 ± 0.08	3.14 ± 0.02	3.39 ± 0.03	3.44 ± 0.02
0.03	2.30 ± 0.16	2.90 ± 0.05	2.71 ± 0.01	2.71 ± 0.02	2.76 ± 0.02
0.04	1.98 ± 0.14	2.51 ± 0.04	2.37 ± 0.01	2.26 ± 0.02	2.31 ± 0.01
0.06	1.56 ± 0.12	1.84 ± 0.04	1.83 ± 0.01	1.66 ± 0.01	1.72 ± 0.01
0.08	1.19 ± 0.10	1.42 ± 0.03	1.41 ± 0.01	1.31 ± 0.01	1.34 ± 0.01
0.1	0.95 ± 0.08	1.17 ± 0.04	1.14 ± 0.01	1.06 ± 0.00	1.08 ± 0.00
0.15	0.66 ± 0.07	0.78 ± 0.04	0.76 ± 0.01	0.74 ± 0.00	0.75 ± 0.00
0.2	0.52 ± 0.06	0.65 ± 0.05	0.60 ± 0.01	0.62 ± 0.00	0.63 ± 0.00

Table 10: Comparison of the acceptance corrected FSR rate per 1000 hadronic events with the predictions of the matrix element calculations. The error on the data is the total error. The error on the GNJETS prediction for $\alpha_s = 0.118$ includes systematic errors. The other errors are statistical only. For $\alpha_s = 0.177$, GNJETS can only be used for $y_{cut} \geq 0.01$.

inclusive particle distributions or the event shape variables where a change in the parton shower can be compensated for by a change in the hadronisation parameters. On the contrary, FSR photons are not sensitive to hadronisation effects. Since the photon emission in the parton shower is fully constrained by the modelling of gluon emission, the comparison between different variants of JETSET is indicative of how higher order corrections are to be implemented into the models. For instance, the surprisingly good agreement of the ‘‘Constant α_s ’’ variant might give a handle on the choice of the evolution variable which governs the running of α_s in the parton cascade.

6.3 Comparison with Matrix Element Calculations

An $O(\alpha_s^n)$ QCD calculation of the $\gamma + n$ jet rates as a function of y_{cut} has been provided by Kramer and Lampe at parton level [3]. This calculation employs a recombination scheme where all final state particles including the photon are treated on the same footing. However, in this analysis, the isolated photon is initially separated from the other particles for the jet reconstruction which together with the cuts employed at parton level implies a different definition of the relevant phase space.

Recently, two Monte-Carlo generators have been made available : GNJETS [6], based on the calculation by Kramer and Lampe [3], and a generator based on a calculation by Glover and Stirling [4] (GS). Both generators can incorporate the cuts used to express the corrected FSR rate. They are expected to give more reliable results for higher values of y_{cut} .

The predictions of the matrix element calculations are given in table 10 and compared with the data in figure 19 and figure 20.

The GNJETS predictions depend on the value of α_s , (taken as a non-running cou-

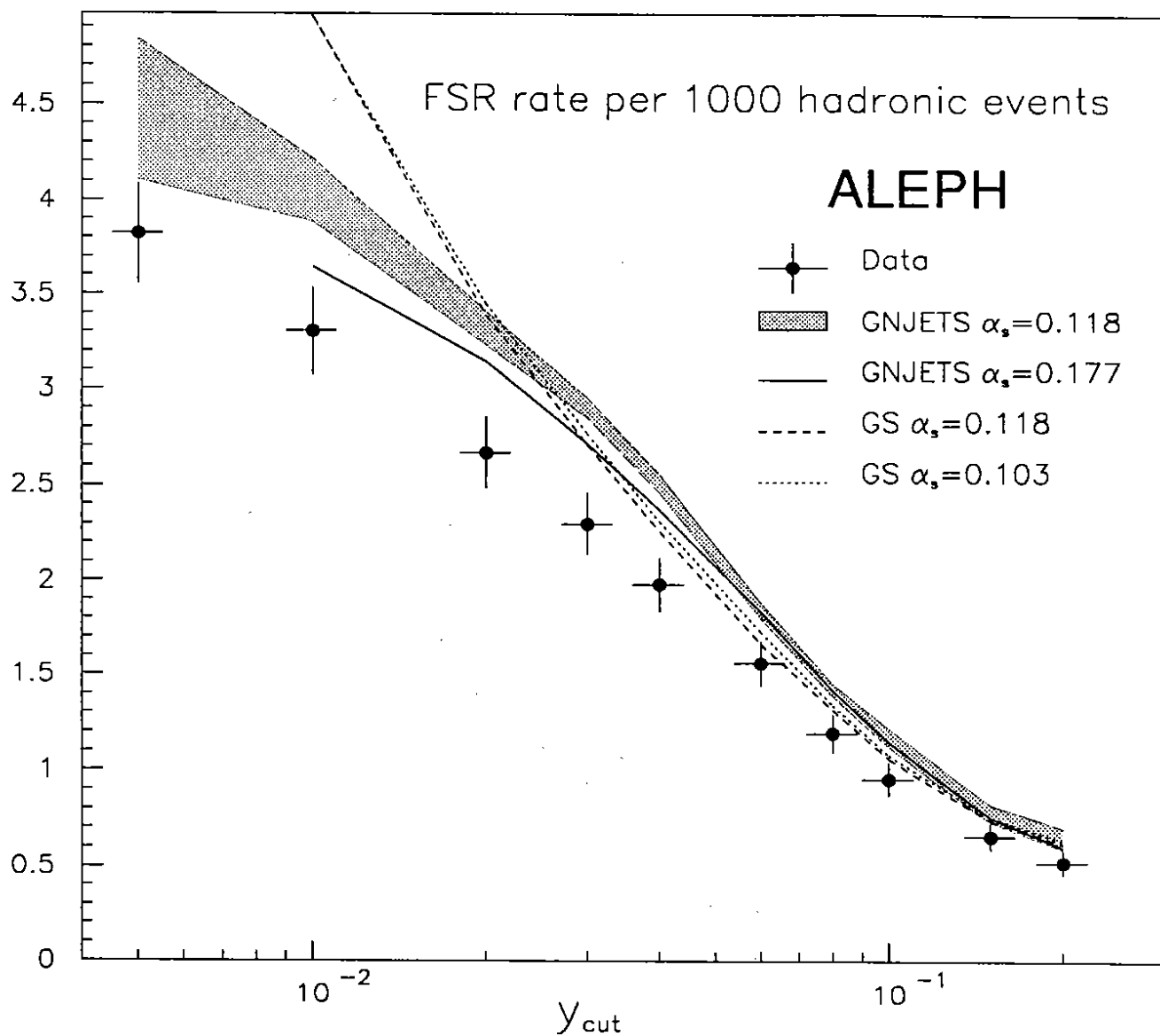


Figure 19: The acceptance corrected FSR rate as a function of y_{cut} and its comparison with matrix element calculations. The band around the GNJETS prediction corresponds to the range given by the variations of the cut-off parameters.

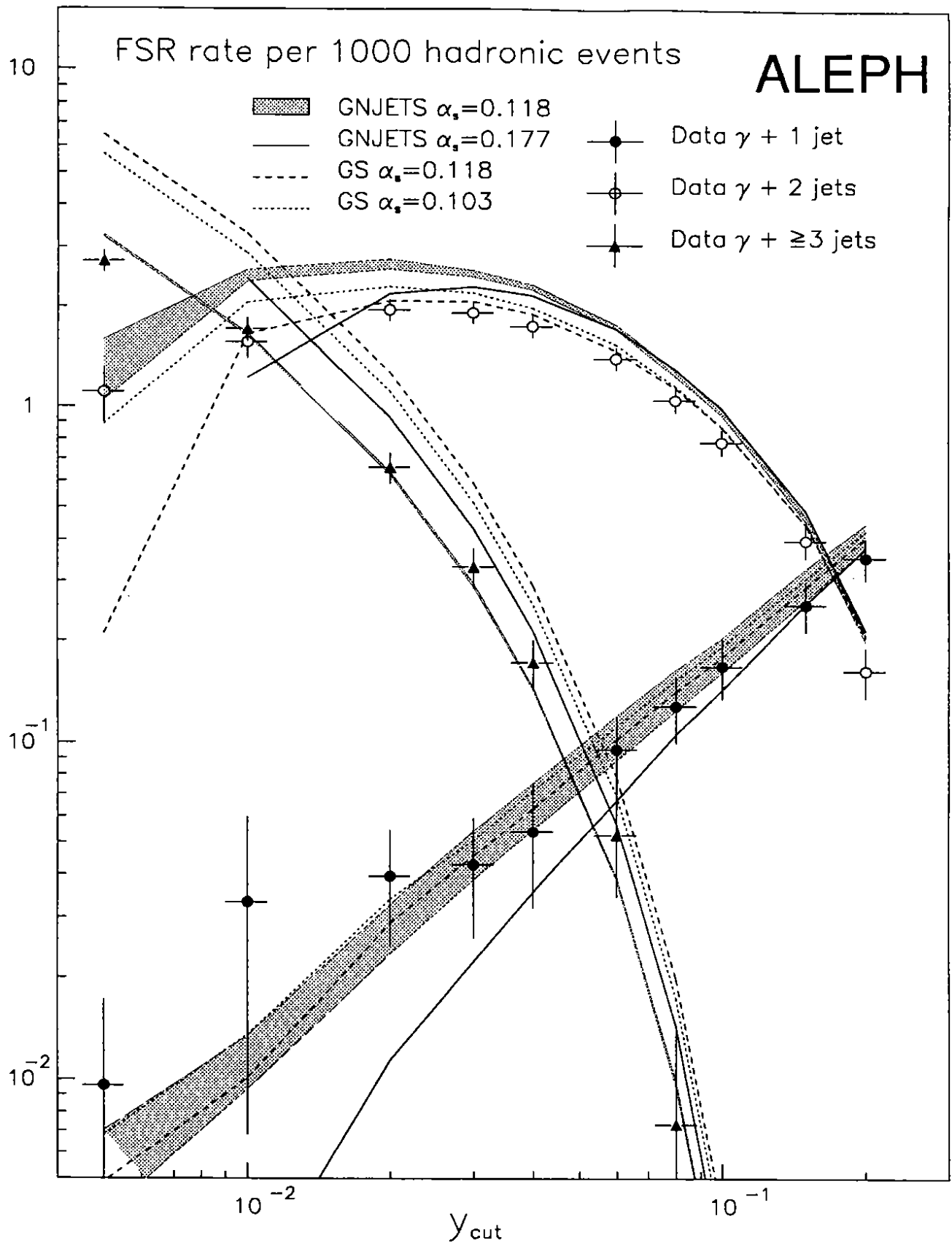


Figure 20: The acceptance corrected $\gamma + n$ jet rates as a function of y_{cut} and their comparison with matrix element calculations. The bands around the GNJETS predictions correspond to the range given by the variations of the cut-off parameters.

pling) and on two intrinsic cut-off parameters [20]. The GNJETS predictions are given for $\alpha_s = 0.118$, which is a value determined in second order QCD [3], and for $\alpha_s = 0.177$, corresponding to first order QCD only [16]. The predictions for the total FSR rate, the $\gamma + 1$ jet rate and $\gamma + 2$ jet rate are sensitive to the values of the cut-off parameters. The effect of changing the value of α_s is comparable with the effect of changing these cut-off parameters.

The GNJETS prediction for $\alpha_s = 0.118$ overestimates the total FSR rate as a function of y_{cut} by 15 to 20% except at high y_{cut} where it agrees with the data. The discrepancy between the data and the GNJETS prediction comes from the $\gamma + 2$ jet rate (figure 20).

The predictions of the GS calculation depend on the running coupling constant derived from the value of Λ and y_{min} , a single cut-off parameter which represents the finite resolution of a hypothetical parton detector. In this analysis, the predictions are insensitive to the choice of y_{min} over the full y_{cut} range [21]. Except at high y_{cut} , the GS prediction differs significantly from GNJETS. The total rate predicted by GS is in good agreement with the data for $y_{cut} > 0.06$ but the prediction for the $\gamma + \geq 3$ jet rate is systematically too high.

7 Conclusions

A clear signal of prompt photons in hadronic Z decays is obtained from a sample of 1336 isolated photons with $E_\gamma > 5$ GeV. The efficiency of the photon identification and the isolation probability are measured using the data. The main systematic error comes from the subtraction of the non-prompt background.

The FSR signal is corrected for both detector and hadronisation effects and is expressed at parton level where $E_\gamma > 5$ GeV, $|\cos \theta_\gamma| < 0.95$ and the summed energy inside a 20° cone around the photon is less than 500 MeV. These corrections introduce a theoretical error comparable with or smaller than the experimental error.

The FSR rate and the $\gamma + n$ jet rates have been measured as a function of y_{cut} and the differential FSR rate is given as a function of both photon energy and p_\perp with respect to the thrust axis for $y_{cut} = 0.005$, $y_{cut} = 0.06$ and $y_{cut} = 0.2$.

The comparison of the measured FSR rate as a function of y_{cut} with the parton shower models indicates that the JETSET prediction is three standard deviations too low at low y_{cut} while the ARIADNE prediction is two standard deviations too high at high y_{cut} . The HERWIG prediction lies within one to two standard deviations of the data. All three parton shower models have difficulties in describing the $\gamma + n$ jet rates as a function of y_{cut} . However, a good agreement between JETSET and all measured rates as a function y_{cut} is found if there is no matrix element matching at the first branching or if a non-running strong coupling is used.

The data are reproduced well by the matrix element calculations of Spiesberger and of Glover and Stirling at high y_{cut} only. The $\gamma + 1$ jet rate as a function of y_{cut} is well described by both calculations but the Spiesberger prediction is too high for the $\gamma + 2$ jet rate while the Glover and Stirling prediction is too high for the $\gamma + \geq 3$ jets rate.

Using FSR photons, the physics of parton cascades can be tested in a unique way. At this time, none of the established parton shower models gives a fully adequate description

of the data.

Acknowledgements

We wish to thank our colleagues in the CERN accelerator division. We are grateful to the engineers and technicians in all our institutions for their contribution towards ALEPH's success. We thank N. Glover, Z. Kunszt, L. Lönnblad, M. Seymour, T. Sjöstrand, H. Spiesberger and J. Stirling for their help and suggestions at various stages of this analysis. Those of us from non-member countries thank CERN for its hospitality.

References

- [1] E. Laermann et al., Nucl. Phys. B 207 (1982) 205.
K. Koller et al., Z. Phys. C 2 (1979) 197.
- [2] Proceedings of the Workshop on Photon Radiation from Quarks, December 2-3, 1991, Annecy, CERN Report 92-04.
- [3] G. Kramer and B. Lampe, Phys. Lett. B 269 (1991) 401.
- [4] N.W.N. Glover and W.J. Stirling, University of Durham Centre of Particle Theory preprint number DTP 92-52.
- [5] Z. Kunszt and Z. Trócsányi, Preprint ETH-TH/92-26.
- [6] G. Kramer and H. Spiesberger, contribution to the Workshop on Photon Radiation from Quarks, December 2-3, 1991, Annecy, Preprint DESY 92-022. GNJETS, Version 2.2, May 20, 1992.
- [7] T. Sjöstrand, Comp. Phys. Comm. 39 (1986) 347; JETSET, Version 7.2.
T. Sjöstrand, contribution to the Workshop on Photon Radiation from Quarks, December 2-3, 1991, Annecy, Preprint CERN-TH.6369/92.
- [8] U. Petterson, LU TP 88-5 (1988), U. Petterson, L. Lönnblad, LU TP 88-15 (1988), L. Lönnblad LU TP 89-10, L. Lönnblad, ARIADNE3.2,
L. Lönnblad, contribution to the Workshop on Photon Radiation from Quarks, December 2-3, 1991, Annecy.
L. Lönnblad, Preprint DESY 92-046, submitted to Comp. Phys. Comm.
- [9] G. Marchesini and B.R. Webber, Nucl. Phys. B 310 (1988) 461.
G. Marchesini, B.R. Webber, G. Abbiendi, I.G. Knowles, M. H. Seymour and L. Stanco, Comp. Phys. Comm. 67 (1992) 465.
M. H. Seymour, contribution to the Workshop on Photon Radiation from Quarks, December 2-3, 1991, Annecy, Preprint Cavendish-HEP-91/17.
- [10] G. Marchesini and B. R. Webber, Nucl. Phys. B 238 (1984) 1.
- [11] D. Decamp et al., ALEPH Collaboration, Preprint CERN-PPE/92-62, to be published in Z. Phys. C.
D. Decamp et al., ALEPH Collaboration, Update submitted to the 26th International Conference on High Energy Physics, Dallas, Texas, August 6-12, 1992.

- [12] D. Decamp et al., ALEPH Collaboration, Phys. Lett. B 264 (1991) 476.
- [13] D. Decamp et al., ALEPH Collaboration, Nucl. Inst. and Meth. A 294 (1990) 121.
- [14] D. Decamp et al., ALEPH Collaboration, Phys. Rep. 216 (1992) 253.
- [15] W. Bartel et al., JADE Collaboration, Z. Phys. C 33 (1986) 23; S. Bethke et al., JADE Collaboration, Phys. Lett. B 213 (1988) 235.
- [16] M.Z. Akrawy et al., OPAL Collaboration, Phys. Lett. B 246 (1990) 285.
G. Alexander et al., OPAL Collaboration, Phys. Lett. B 264 (1991) 219.
P.D. Acton et al., OPAL Collaboration, Z. Phys. C 54 (1992) 193.
- [17] J.E. Campagne and R. Zitoun, Z. Phys. C 43 (1989) 469.
- [18] M. Seymour, Preprint Cavendish-HEP-91/16, to appear in Z. Phys. C.
- [19] B. Kniehl, contribution to the Workshop on Photon Radiation from Quarks, December 2-3, 1991, Annecy.
- [20] The cut-offs Y_{MIN} and Y_{PMIN} have been set to 0.001. The error band around the GNJETS predictions for $\alpha_s = 0.118$ corresponds to variations in Y_{MIN} between 10^{-5} and 0.005 and variations in Y_{PMIN} between 10^{-4} and 0.005.
- [21] The parameter y_{min} is chosen such that $y_{min}/y_{cut} \leq 0.01$.